Past, present and future subrosion rates of the Ternaard diapir

Internship report for COVRA N.V. by Sophie de Nonancourt (0797766)

Supervised by Jeroen Bartol (COVRA N.V.) and Liviu Matenco (Utrecht University)

ABSTRACT

Radioactive waste results from a wide variety of activities, including the generation of energy and production of medical isotopes. Following temporary above ground storage, geological disposal in a stable geological formation of the radioactive waste is foreseen. Currently, the Netherlands is considering selecting a disposal method and site for radioactive waste around 2050. One of the host rocks currently under consideration is rock salt: a bedded and domal rock salt (diapir). Subrosion has the ability to reduce the thickness of the rock salt separating waste from surrounding sediments and groundwater over time. It is therefore important to understand the temporal evolution of subrosion and its impacts on the salt diapir, as the integrity of the salt barrier is crucial. If subrosion occurs too fast, it could compromise the containment of the waste, leading to the premature release of radionuclides that haven't sufficiently decayed into the environment, which poses long-term risks to both the environment and human health.

This study focuses on the Ternaard diapir, a relatively shallow diapir with a thin caprock, located in north Friesland. To understand and quantify its evolving subrosion rates, we use seismics, salt-budget analysis as well as zero-dimensional reactive-transport model (Phreeqc) for a range of Darcy fluxes ($1 \times 10^{-6} - 5 \times 10^{-3}\ m/yr$), inflow water chemistries and caprock thicknesses (0, 13 and 65 m).

Results from the salt budget analysis indicate an average subrosion rate of 5.9 m/myr since the last 23 million years ago, in line with the modelling results. Furthermore, the modelling results show that caprock presence has the strongest limitation on the subrosion rate, whereas groundwater composition and flow magnitude introduce smaller but systematic variations: fresher water and higher groundwater fluxes result in higher subrosion rates.

TABLE OF CONTENTS

1. INTRODUCTION

Radioactive waste is generated by a wide range of societal activities, such as energy production or the manufacturing of medical isotopes. After a period of temporary above-ground storage, long-term isolation of this waste is envisaged through geological disposal in stable geological formations. In the Netherlands, a decision on the disposal method is currently foreseen around 2050 (COVRA. N.V., 2024). Among the host rocks under consideration is rock salt: a bedded and domal rock salt (diapir). Rock salt is regarded as a favorable disposal medium because of its low permeability, self-healing behavior and mechanical stability (Jackson & Hudec, 2017; Li et al., 2024). However, salt structures are susceptible to subrosion, whereby undersaturated groundwater dissolves halite and progressively reduces the thickness of salt separating the waste from surrounding sediments and groundwater over time (Sanford, 1992; Auzemery et al., 2025). Understanding the temporal evolution of subrosion and its impact on salt diapirs is therefore critical for assessing the long-term integrity of such host-rock (Li et al., 2024). Maintaining an effective salt barrier is critical, as the containment of the repository would be compromised if subrosion occurs too quickly. A rapid breach would allow radionuclides to escape into the groundwater before their radioactivity has sufficiently decayed; once they reach the surface environment, these high-activity isotopes pose severe long-term risks, such as ionizing radiation damage to DNA, to both environment and human health (COVRA. N.V., 2024).

The Ternaard diapir is a shallow Zechstein salt structure situated at the transition between the onshore Friesland aquifer system and the brackish hydrology of the Waddenzee (NLOG., 2023; Fig. 1), making it a particular diapir to research, as few diapirs in the Netherlands currently occupy such a transitional position and have been subjected to a history of exposure to topography-induced meteoric flushing during sea-level minimums (Appelo & Postma, 2005). Its crest lies at approximately -615 m depth, making it one of the shallowest diapirs in north Friesland (TNO, 2014). Seismic and well data show that Ternaard is predominantly halitic and internally homogeneous, characteristic of the large mature salt domes of Friesland and Groningen (Van Gent et al., 2011; Lauwerier, 2022). A key feature of the diapir is its unusually thin caprock (~13 m), which contrasts sharply with neighbouring structures such as the Pieterburen diapir, where caprock thickness reaches ~90 m (García-Monzón et al., 2022). This variability suggests strong spatial differences in long-term subrosion intensity across short distances (Auzemery et al., 2025). The limited caprock development at Ternaard, despite its shallow position, indicates a comparatively moderate cumulative dissolution history and highlights the diapir's transitional hydrological setting (Auvray et al., 2023).

The aim of this study is to understand and quantify Ternaard's evolving subrosion rates, by gathering past, present and expected future subrosion rates. To reach this goal, seismic interpretation of the diapir is performed using Petrel, a seismic interpretation software. With the results stemming from the interpretation, the salt budget based on the method of Zirngast (1996) will be calculated and from it, the past rates from the last 100 million years ago are

inferred. Additionally, based on a model by Li et al. (2024), a zero-dimensional model was built, using PHREEQC (geochemical modelling software), to establish present and future halite dissolution rates at Ternaard, for a range of Darcy fluxes ($1 \times 10^{-6} - 5 \times 10^{-3}\ m/yr$), groundwater inflow fluid chemistries (based on aquifer composition from Griffioen et al., 2016) and caprock thicknesses (0m, 13m and 65m). The results will then be compared to data from other diapirs, as well as the results from the salt budget to attempt to understand further the drivers of subrosion at Ternaard.

2. GEOLOGICAL BACKGROUND

2.1 Regional Geological evolution of the Dutch Zechstein diapirs

The northern Netherlands, including the Friesland Platform (Fig. 1), is underlain by a geological history defined by repeated cycles of crustal extension and compression. This tectonic activity established the structural framework that controlled the deposition, mobilization, and entrapment of the Permian Zechstein salt (Lauwerier et al., 2022).

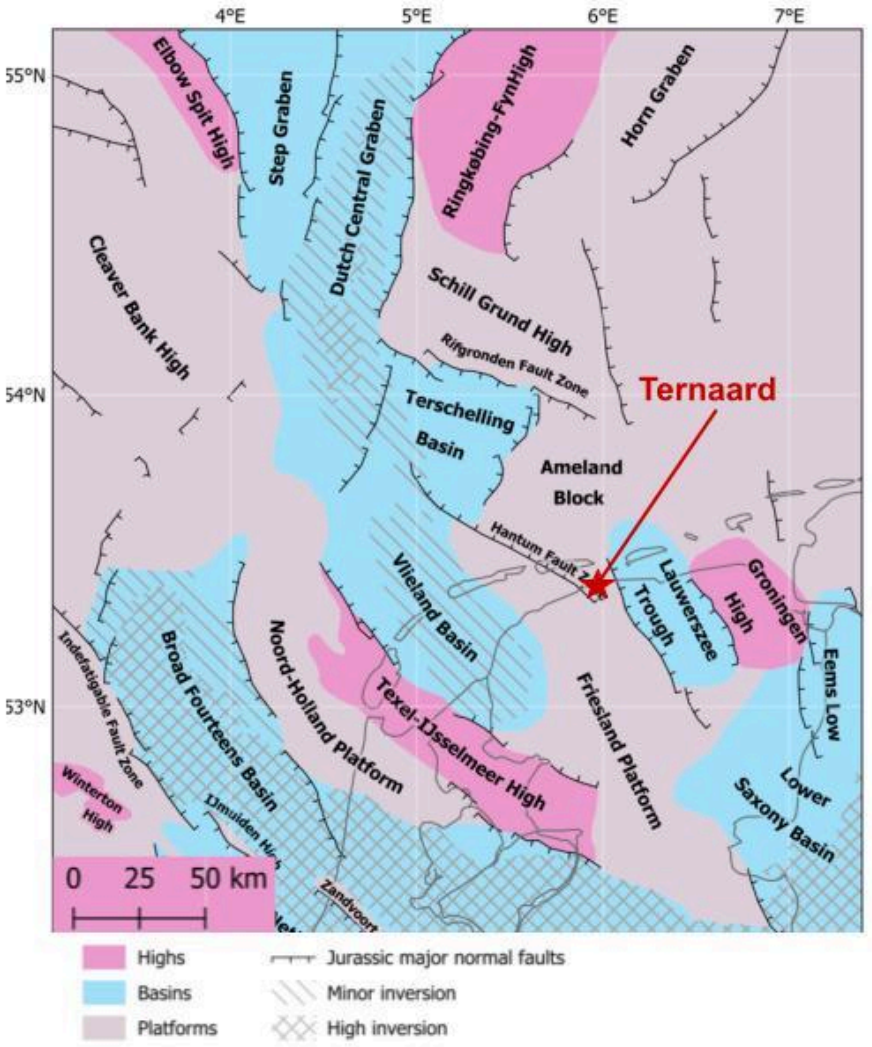

Figure 1: Regional structural map of the Southern North Sea and northern Netherlands delineating the distribution of tectonic highs, basins, and platforms. The red star indicates the Ternaard diapir location, which is the study area of interest for this report (Picture retrieved and adapted from Weert et al., 2025).

This framework originated during the assembly of the supercontinent Pangea. During the Devonian and Carboniferous, the Variscan Orogeny, the collision of Gondwana and Laurussia, created a network of deep-seated, northwest-striking faults and zones of crustal weakness that exerted control on later deformation (Verweij, 2003; Doornenbal & Stevenson, 2010). By the Early Permian, the region was situated within the arid interior of the Pangean landmass. Regional thermal uplift and erosion (the Saalian phase) formed the Base Permian Unconformity (Verweij, 2003), followed by thermal subsidence that created the Southern Permian Basin, which was initially filled with the Rotliegend Group (~299-257 Ma).

During the Late Permian (~257 Ma), the Zechstein transgression occurred as a rise in eustatic sea level breached the Barents Shelf, flooding the Pangean interior with North Atlantic waters. This was not a single event but a series of high-frequency transgressions and regressions that defined the Zechstein Group (Geluk., 2007). During transgressive phases, the basin was recharged with marine water, depositing carbonates (e.g., the Zechstein Limestone). During subsequent regressions or periods of restricted inflow, intense evaporation in the arid climate led to the retreat of the sea, triggering the precipitation of sulfates and thick halite sequences. These repeated cycles resulted in five distinct evaporitic sequences (Z1-Z5), reaching a thickness of 600-800 m on the Friesland Platform, a volume of salt necessary for the initiation of future salt tectonics (De Jager, 2007; Peryt et al., 2010; Lauwerier, 2022).

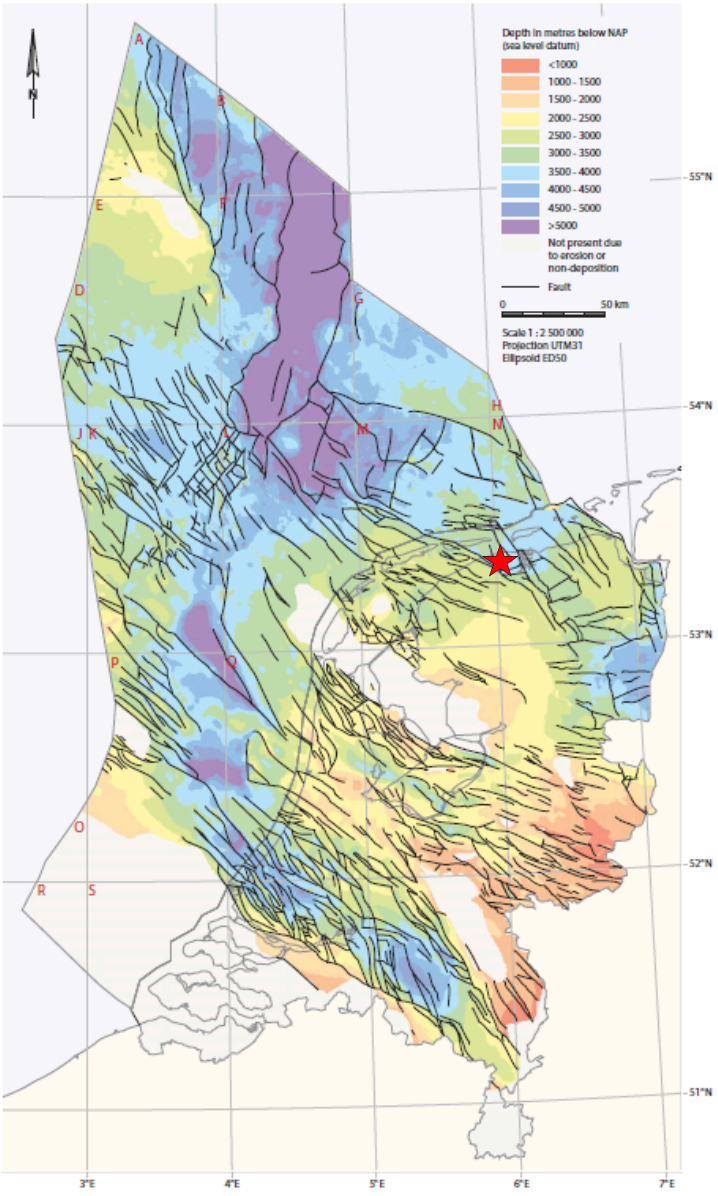

Figure 2: Depth map of the Zechstein Group (Late Permian), figure retrieved from Duin et al. (2006). Ternaard (represented by a red star) is located on a stable structural high, where the Zechstein depth is lower (2500-4000m depth) than in neighbouring basins, such as towards the Lower Saxony Basin (Fig. 1; >3500 m depth).

Initial salt movement began in the Triassic as Pangea began to experience early rifting and internal tension. This movement was driven by differential loading from the deposition of the Lower Germanic Triassic Group (RB) (~252-247 Ma) and the Upper Germanic Triassic Group (RN) (~247-208 Ma), alongside extensional tectonics linked to the northward propagation of the Tethys rift system (Stewart et al., 2007). While the Ternaard structure began as a salt pillow during this phase, the trigger for diapirism on the stable Friesland Platform was a Middle Jurassic regional uplift event known as the Mid-Kimmerian phase (Verweij, 2003). This doming caused erosion of the overlying Triassic and Altena Group (AT) (~200-155 Ma) sediments across the platform. The resulting thinned overburden, which contrasted with the thicker sequences preserved in adjacent basins, created a differential load that initiated and accelerated salt withdrawal into pillows and early piercement structures (Van den Haute & Vercoutere, 1990; De Jager, 2007).

A phase of crustal extension during the Late Jurassic to Early Cretaceous (the Kimmerian rift phase) further reactivated deep faults and increased heat flow (Verweij, 2003). This regime amplified salt movement during the deposition of the Niedersachsen Group (SK) (~152-140 Ma) and the Rijnland Group (KN) (~140-100 Ma), as salt exploited thinned sediment and fault-controlled weaknesses to form mature salt walls and diapirs (Ten Veen et al., 2012). During this time, the Ternaard diapir developed into a piercement structure. While this period caused inversion and erosion in neighboring rift basins, the Friesland Platform experienced milder compression during the Late Cretaceous Subhercynian and Laramide phases (De Jager, 2007; Lauwerier, 2022). This stability allowed for the deposition of a continuous Chalk Group (CK) (~100-66 Ma) seal, preserving the salt structures. From the Paleocene onward, the region subsided under the weight of the North Sea Supergroup (U/M/LNSG; comprised respectively of the Upper, Middle and Lower North Sea groups), which buried and stabilized the Ternaard diapir (Fig. 1) into its current configuration (Verweij, 2003).

2.2 Salt composition, diapir mechanics and Subrosion processes

The Zechstein evaporite sequence is heterogeneous, organized into five main evaporitic cycles (Z1 through Z5) that reflect the progressive evaporation and replenishment of the Zechstein Sea. While massive halite dominates the sequence, particularly within the thick Z2 (Stassfurt) and Z3 (Leine) cycles, it is interbedded with varying volumes of anhydrite, dolomite, claystone, and halitic clay throughout this cyclic structure (Geluk, 2007; Storzyk et al., 2014). This lithological complexity is not only stratigraphic; it governs the internal deformation, permeability, and mechanical behaviour of the resulting diapirs. The proportion of these less soluble impurities varies regionally, with northern onshore diapirs typically comprising 2-8% non-salt lithologies, while their eastern counterparts can contain substantially more (Strozyk et al., 2014).

The long-term evolution and structural stability of these diapirs are influenced by subrosion, the process of halite dissolution by groundwater contact. Modelling and field data indicate that dissolution is highly focused at diapir crests and shallow flanks, where hydraulic

gradients are strongest (Lauwerier et al., 2022). Additionally, dissolution rates are strongly lowered with depth due to decreasing hydrological connectivity (Sanford, 1992; Auvray et al., 2023). As the halite is removed, the insoluble residues accumulate, forming a caprock composed of anhydrite, gypsum, carbonates, and clay. The thickness of this protective layer exhibits regional variation, from a few metres in offshore settings to over 80 metres in shallow onshore diapirs subjected to further freshwater circulation (García-Monzón et al., 2022).

The intensity of subrosion is, in part, dictated by the groundwater flow regime. National hydrological models, such as REGIS II and the National Hydrological Instrument (NHI), reveal steep hydraulic gradients and active meteoric flow in the northern onshore region. This is particularly true within the Pleistocene aquifers that directly overlie many diapirs (Rijkers & Duin, 1994). On the other hand, offshore hydrodynamic conditions are characterised by weaker gradients and less permeable aquifer systems, which reduce dissolution potential. This leads to the preferential preservation of thick, relatively undeformed halite masses (Roodhart, 1987). This contrast in hydrogeology explains the systematic regional patterns observed in caprock thickness, modern dissolution rates and overall diapir morphology.

3. METHODOLOGY

This study integrates seismic interpretation to determine the subrosion rates through time (see section 3.1), quantitative salt-budget reconstruction (see section 3.2), and 0D geochemical-transport modelling (see section 3.3) to evaluate halite subrosion rates under different hydrological and chemical boundary conditions.

3.1 Seismic interpretation

The subsurface geometry used in this paper is derived from publicly available 2-D reflection seismic data and well tops retrieved from the Dutch national subsurface database (NLOG.NL, managed by TNO). The following seismic lines and wells were used for the seismic interpretation, performed in Petrel: the lines L3NAM2015AR, L3NAM2009BR, L3NAM2016AR and the well TNR-01. Following the methodological approach of Lauwerier (2022), based off of Zirngast's (1996), seismic reflectors were tied to stratigraphic group boundaries using additionally well logs (surrounding deep and shallow wells used in the Digital Geological Model) that had previously been converted to the time domain, as part of a previous Petrel project done by the Utrecht University Tectonics Group. Reflectors corresponding to the Zechstein Group boundaries and major post-Zechstein horizons were mapped across the survey area to delineate the diapir and other sediment layers present. Indeed, the North Sea and Chalk groups were selected for the salt budget analysis because they represent the primary post-rift overburden sequence where thickness variations directly reflect salt withdrawal and diapiric growth, whereas the older Triassic and Jurassic strata were significantly truncated or redistributed by the Mid-Kimmerian regional uplift (Verweij, 2003; De Jager, 2007).

3.2 Calculating the Salt Budget

The salt budget reconstruction follows the basin-scale 3D volumetric approach outlined by Zirngast (1996) and applied to the Dutch diapirs by Lauwerier (2022) and Almalki (2023). Thickness variations in syn-kinematic stratigraphic units were used to quantify salt withdrawal into the diapir and temporal evolution of the diapir growth (Fig. 3).

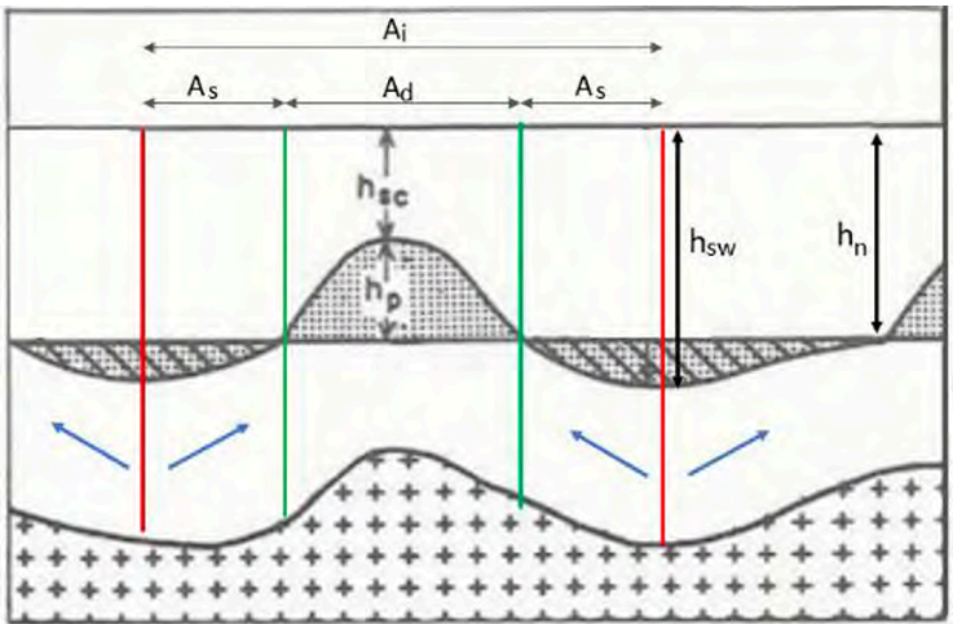

Figure 3: A schematic cross-section illustrating the relationship between a salt dome and adjacent withdrawal basins. Key geometric parameters include the total influence area (A_i), which consists of the central dome area (A_d) and the flanking salt source areas (A_s). Variations in sediment thickness due to salt movement are defined as h_n (normal regional thickness), h_{sw} (maximum thickness within the withdrawal basin), and h_{sc} (minimum thickness directly above the dome). The height of the diapir is represented by h_p, while blue arrows denote the direction of salt flow from source areas into the dome. This figure is retrieved from Lauwerier et al. (2022), who adapted it from Seni & Jackson (1984).

For each stratigraphic interval of interest, the following steps were performed:

- Determining the thickness of sediment deposited within the salt withdrawal basin (h_{sw}) from the interpreted seismic horizons.
- Establishing the normal sediment thickness (h_n) as a proxy for regional, non-salt-related subsidence.
- Delineating the main area of diapiric influence (A_i), salt source areas (A_s) and domal areas (A_d) based on where sediment thickness, relative to h_n, indicated

withdrawal or thinning, respectively. The main area of diapiric influence was delineated by identifying the boundary where the Zechstein salt layer became extremely thin, typically where the maximum sediment thickness was observed on the thickness maps of the stratigraphic intervals affected by salt tectonics (Lauwerier et al., 2022).

The withdrawn salt volume (V_s) was then calculated by multiplying the excess sediment thickness by the source area: $V_s = (h_{sw} - h_n) \times A_s$. This volume was converted to an equivalent column height (c_t) by normalising V_s over the domal area: $c_t = V_s/A_d$. Subsequently, the difference between this calculated maximum potential column height and the actual salt column height (c_a), determined from the sediment thickness above the dome (h_{sc}), yielded the eroded or subroded column height (c_e), such as $c_e = c_t - c_a$. The actual net growth (c_a) was calculated as the difference between the mean regional sediment thickness (h_n) and the thickness of the sediments preserved directly above the diapir (h_{sc}). Finally, the subrosion rate ($c_e/\Delta T$) from the interval of duration ΔT were derived, providing the volume loss over the last 100 million years.

3.3 0D modelling: subrosion rate

3.3.1 Geochemical model setup

To quantify subrosion under variable hydrological and geological conditions, a series of zero-dimensional simulations was run, using the geochemical software PHREEQC (Interactive version, software developed by David Parkhurst and Tony Appelo). The system was conceptualized as a closed batch reactor containing a fixed mass (in excess) of halite in contact with a finite volume of reactive fluid (Fig. 4), representing the composition of the groundwater overlying the diapir's crest at 615 m depth. To better highlight the structural evolution of the Ternaard diapir, the modelling approach distinguishes between two primary regimes: an interface-controlled regime and a transport-limited regime. For the "no caprock" (0 m caprock thickness) scenarios, the model simulates the direct contact between the halite surface and the aquifer, consistent with the batch salt reactor methodology applied by Li et al. (2024) for Zechstein salt facies. On the other hand, the "caprock" (13 m or 65 m caprock thickness) scenarios were adapted to follow the conceptual framework of Auzemery et al. (2025), modified here for 0D modelling, where the caprock acts as a stagnant hydraulic and diffusive buffer. By transitioning between these regimes, the objective was to quantify the sensitivity of halite dissolution rates to Darcy flux, groundwater fluid salinity, and the physical protection created by a caprock. To ensure technical reproducibility and numerical consistency across all runs, a constant bulk surface area (A_{bulk}) of 1000 m² was utilized. This area allows the regional Darcy flux (q) to be scaled into a manageable annual volumetric fluid throughput (e.g., q = $1 \times 10^{-6}\, m/yr$ yields 0.001 m^3/yr or 1 kg of water) for the PHREEQC calculation. Because PHREEQC Interactive does not allow for direct velocity specification, this flux-to-volume

scaling provides the necessary methodology to derive the vertical retreat rate (R in m/yr) from the molar dissolution results.

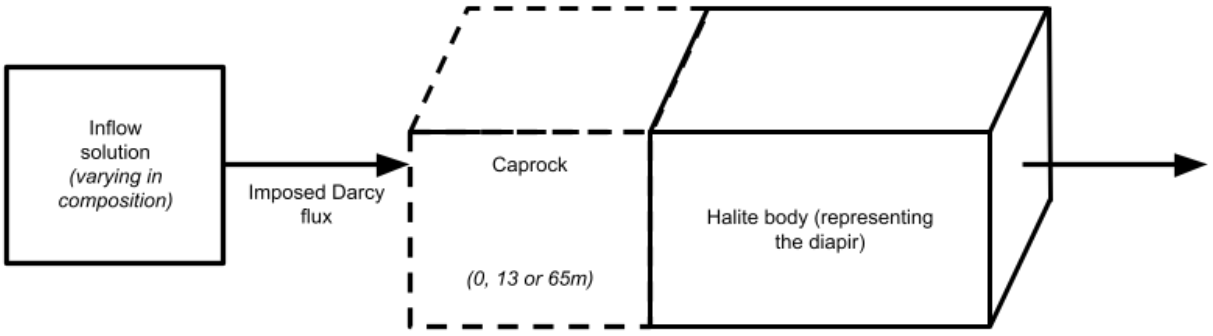

Figure 4: Conceptual model representing 0D geochemical simulations performed in this report aiming to quantify the sensitivity of halite dissolution rates to Darcy flux, fluid salinity, and caprock presence. This model is based and adapted on the model created by Li et al. (2024).

The groundwater fluid was given four different Darcy flux values, ranging from 1×10^{-6} to $5 \times 10^{-3} m/yr$. Those fluxes were chosen to cover the hydrological end-members typically considered in long-term safety assessments and basin-scale studies (Li et al., 2024). The lowest flux ($1 \times 10^{-6} m/yr$) serves as the proxy for deep, nearly stagnant groundwater flow, where transport is dominated by diffusion, while the intermediate values model active regional flow systems. Oppositely, the highest flux ($5 \times 10^{-3} m/yr$) reflects an extreme yet physically plausible high-recharge scenario, potentially linked to glacial meltwater infiltration or fault-enhanced permeability (Li et al., 2024).

Additionally, when testing the effect of the caprock's presence (Fig. 4), two different lengths for the latter were chosen: (1) 13m caprock, chosen to represent the thickness documented for the Ternaard diapir (Auzemery et al., 2025); and (2) 65m caprock, to represent a thicker caprock. The 65m value was selected to approximate the regional average thickness of Zechstein caprocks in the Netherlands, which typically ranges from 40m to 100m in more mature structures (e.g., the Schoonloo or Pieterburen diapirs), therefore allowing for a comparison between the specific thin caprock at Ternaard and a more representative regional case (Lauwerier, 2022; Auzemery et al., 2025). Ultimately, this range of caprock thickness does not fully encompass the known structural variability of Dutch Zechstein caprocks (Auzemery et al., 2025), but the aim of this study was to establish how subrosion evolves as the groundwater's residence time in the caprock increases, in addition to quantifying the influence of salinity and Darcy flux on subrosion rates.

3.3.2 Constraints on the halite dissolution rates

Halite dissolution: Surface-controlled kinetics modelling for a diapir with no caprock

The rate law implemented for halite dissolution follows a kinetic formulation where the net dissolution rate is proportional to the mineral's reactive surface area and the chemical affinity of the solution [1].

$$Rate = k_t * A_t * (1 - \Omega) \quad [1]$$

Where k_t is the temperature-corrected rate constant ($mol\, m^{-2} s^{-1}$), A_t is the total reactive surface area (m^2), and SI is the saturation index of halite. Ω is the saturation ratio, and $(1 - \Omega)$ represents the chemical driving force, ensuring the rate approaches zero as the solution approaches saturation ($\Omega \rightarrow 0$). A temperature correction is essential because dissolution kinetics are strongly temperature-dependent, which is applied using the Arrhenius equation [2] to calculate k_t.

$$k_t = k_{25} * exp[-\frac{E_a}{R}(\frac{1}{T} - \frac{1}{298.15})] \quad [2]$$

The pre-exponential factor $k_{25} = 10^{-0.21}\, mol\, m^{-2} s^{-1}$ and the activation energy $E_a = 7.4\, kJ\, mol^{-1}$ were taken directly from Li et al. (2022). The specific surface area (SSA) is set to 1×10−4 m^2 kg⁻¹, a value also adopted from Li et al. (2022) to represent a realistic effective surface area for subsurface halite. The total reactive surface area A_t in the calculation is the product of this SSA and the current mass of halite (Appendix, Input file. A), to account for the microscopic mineral-fluid interface within the salt matrix, which dictates the kinetic speed of dissolution.

Halite subrosion: Caprock-controlled subrosion modelling

In the presence of a caprock, either 13m or 65m, the rate-limiting step for halite subrosion changes. As observed in Auzemery (2025), the presence of a thick caprock creates a hydraulic decoupling between the aquifer and the salt diapir. While hydraulic gradients may drive water towards the salt, the low permeability of the caprock ensures that mass transport is restricted to diffusion. Therefore, the subrosion rate is modeled as the outward diffusive flux of Na^+ and Cl^- ions through the caprock matrix, rather than the inward advective flow of groundwater. The subrosion rate is modeled as a diffusive flux using the following equation [3], based on Fick's First Law of Diffusion.

$$Rate = \frac{D_{eff}}{L} * A_t * (C_{sat} - C_{current}) \quad [3]$$

Where D_{eff} is the effective diffusion (m^2/s), L is the caprock thickness, A_t is the total reactive surface area (m^2), scaled with the same specific surface area as for the no-caprock simulations by PHREEQC, and ($C_{sat} - C_{current}$) is the chemical driving force between the saturated halite interface and the top of the caprock. The C_{sat} value for halite was retrieved from the Pitzer.dat database (Appendix, Table C). Additionally, to account for the physical constraints of the caprock, the effective diffusion coefficient (D_{eff}; [4]) is derived by correcting the base diffusion (D_0) for porosity (Φ) and tortuosity (τ) of the caprock.

$$D_{eff} = D_0 * \frac{\Phi}{\tau} \quad [4]$$

A base diffusion (D_0) value of $1.6 * 10^{-9} m^2/s$, based on the diffusion coefficient of the $Na^+$and Cl^- ions is used in all the simulations to represent the ions at reservoir temperature of 30℃, and the tortuosity value was set to be equal to 3 (Appelo & Postma, 2005). Ultimately, by adjusting porosity in different scenarios, the model aims to capture the sensitivity of the subrosion rate based on the structural integrity of the caprock.

3.3.3 Input Parameters

Groundwater inflow fluid composition, flow and thermal conditions

In PHREEQC, the geochemical simulations were all performed using the Pitzer.dat thermodynamic database. The geochemical model required defining end-member fluid compositions to capture the chemical control exerted by interacting fluids on halite subrosion. To account for the temporal variability of recharge chemistry, each flux simulation was combined with three groundwater inflow compositions, retrieved from Li et al (2024). These inflow compositions correspond to the typical water chemistry found in three characteristic subsurface environments of the Netherlands: shallow aquifers, deeply buried aquifers, and deep oil and gas reservoirs. Table 1 presents the specific chemical parameters, including pH and the concentrations of aqueous species in mg L^{-1}. The proposed compositions are based on the established work of Griffioen et al. (2016), and the salinity of these modelled fluids ranges from 1 g L^{-1} to 90 g L^{-1}. Temperature-wise, thermal conditions in the model were assigned following the regional Dutch geothermal gradient according to depth. The temperatures of the caprock brine and all groundwater inflow solutions were standardised to 30℃ and the Halite body brine was assigned a slightly higher temperature of 35℃ consistent with its position deeper within the salt structure.

Table 1: Fluid compositions used in the Geochemical model (in mg/L), from Griffioen et al. (2016).

Fluid Type	Temp (°C)	pH	Na	K	Ca	Mg	Cl	SO_4 (as S(6))	HCO_3 (as C(4)/Alkalinity)	H4SiO 4
Shallow aquifers ($\sim 1\ g/L\ salinity$)	**30**	**7.7**	**582**	**25**	**46.5**	**19.8**	**460**	**43.2**	**458**	**15.35**
Deep, buried aquifers ($\sim 9\ g/L\ salinity$)	**30**	**7.5**	**3480**	**67.2**	**106**	**85.1**	**5200**	**93.7**	**595**	**18.5**
Deep Oil and Gas aquifers ($\sim 90\ g/L\ salinity$)	**30**	**6.4**	**30400**	**310**	**3958**	**920**	**59130**	**78.8**	**231**	**102**

Annual fluid volume

To simulate the geochemical evolution of the system over time, the annual fluid volume interacting with the salt must be defined. This volume is determined based on the Darcy flux ($q = 1 \times 10^{-6}\ to\ q = 5 \times 10^{-3}\ m/yr$), representing the regional groundwater flow, and a defined bulk cross-sectional surface area (A_{bulk}) of 1000 m^2. This area was chosen to scale the regional Darcy flux into an annual volumetric fluid throughput (1 kg for the lowest flux) that ensures the PHREEQC solution mass is numerically representative.

Without a caprock: For simulations representing a system without a caprock, the equivalent annual fluid volume passing through the system is calculated by converting the Darcy flux into a total annual volumetric flow rate [5].

$$Annual\ fluid\ volume\ [m^3/yr] = q\ [m/yr]\ *\ A_{bulk}\ [m^2] \qquad [5]$$

This volume was then introduced into the batch reactor as the initial fluid mass in the *SOLUTION* block (Appendix, Input file. A). The system was allowed to react kinetically with halite over a simulated period of one year, after which, if the simulation were to be longer, the fluid would be refreshed to represent continuous advective supply.

With a caprock: In the presence of a caprock (13m or 65m), the caprock acts as a hydraulic and diffusive buffer (Auzemery et al., 2025). While the Darcy flux still defines the total volume of water moving through the overlying aquifer system, the low permeability of the caprock restricts direct advective contact with the salt. The annual fluid volume is calculated using the same equation [5] as for the simulations with a caprock present. However, in these simulations, the interaction at the salt-caprock interface is mediated by the caprock's effective porosity (Φ = 1% or 10%). This porosity dictates the pore volume available for diffusive

transport. To reflect the specific mineralogical environment of the Ternaard salt structures, the groundwater inflow fluid was equilibrated with a mineral assemblage (Anhydrite, Gypsum, Calcite, and Dolomite) using the *EQUILIBRIUM_PHASES* block before halite dissolution began (Appendix, Input File. B). This step makes sure that the fluid reaching the salt interface is already saturated with respect to the common sulfate and carbonate minerals found within the Dutch Zechstein caprocks (Lauwerier, 2022).

3.3.4 Output Measurements

At the end of each simulation, an output file is created by PHREEQC and the information in that file is printed following the steps from the *SELECTED_OUTPUT* and *USER_PUNCH* blocks (Appendix, Input file. A-B). Equation [6] showcases the calculation PHREEQC did to retrieve the halite dissolution rate ($in\ mm/yr$).

$$subrosion\ rate\ (mm/yr) = \frac{moles\ dissolved\ in\ one\ year\ [mol] * Halite\ Molar\ Mass\ [kg/mol]}{Halite\ density\ [kg/m^3] * S_{cell}\ [m^2]} * 1000 \quad [6]$$

Where S_{cell} varies based on the scenario, to accommodate the specific transport physics being modeled. Following the approach of Li et al. (2024), the no-caprock scenarios are modeled as a batch salt reactor where groundwater inflow fluid directly interacts with the salt; here, S_{cell} is set to $1\ m^2$, representing a unit surface area, where dissolution occurs across the exposed salt-water interface without being restricted by caprock permeability. On the other hand, the caprock scenarios transition into an interface-controlled model where transport physics are explicitly taken into account. In these cases, a larger bulk surface area ($S_{cell} = 1000\ m^2$) is used to better reflect the spatial extent of the porous caprock and the resulting diffusive flux across the diapir's crest. It is important to note that this model distinguishes between the microscopic and macroscopic scales of the interface. While the total reactive surface area (A_t) is a kinetic parameter that accounts for the microscopic texture of the halite and controls the speed of the chemical reaction, S_{cell} defines the physical geometric boundaries, either unit or bulk, used to measure the vertical retreat. Despite these different initial areas, the final calculation [Eq. 6] divides the total mass loss by the respective S_{cell} value. This normalization step effectively converts both scenarios into the same "unit area" basis. This ensures that while the caprock model accounts for larger-scale transport physics, the final impact is reported as a standardized physical retreat of the interface level ($mm/yr\ or\ cm/Myr$), allowing for a direct comparison between the advective dissolution of unprotected salt and the diffusive subrosion of protected salt structures.

4. RESULTS

4.1 Seismic Interpretation of the Ternaard diapir

To perform the salt budget calculations and sensitivity analysis on past subrosion rates, the seismic interpretation of the subsurface had to be executed. A total of 7 stratigraphic groups were delineated (Fig. 5a & 5b), using specific reflectors, as detailed in table 3.

From the seismic interpretation (Fig. 5a & 5b), the Ternaard diapir showcases a broad, asymmetric domal structure with a pronounced NW-SE elongated trend (Fig. 5a & 5b). The top of the diapir is characterized by a single, eccentrically located culmination towards the N-E, where elevation increases rapidly, producing a relatively steep flank. Away from this high, the diapir's flanks slope more gradually towards the S-W, which results in gentler and more extensive slope. This asymmetry results in a tilt from NE to SW, reflecting non-uniform salt rise and withdrawal during diapiric growth, which is likely influenced by pre-existing basement faults (Verweij, 2003). The top of the diapir is smooth but not flat, with minor secondary highs and shallow depressions. This is likely due to differential subrosion or internal salt flow (Strozyk et al., 2012). Ultimately, the overall geometry suggests lateral variability in salt withdrawal and possibly caprock development, which is a configuration that can lead to heterogeneous subrosion and groundwater flow pathways (Appelo & Postma, 2005).

For the delineation of the diapir, the Zechstein Group serves as the primary salt layer for this study, characterized by a very strong negative reflector at its base that is highly faulted (Fig. 5a & 5b). Seismic profiles reveal the internal salt facies to be chaotic and transparent, where halite flow has wrapped around deformed, high-amplitude reflectors interpreted as anhydrite banks (Strozyk et al., 2012, Fig. 5a & 5b). The intra-salt layers have been deformed and partially dispersed during halokinesis, which reflects ductile flow within the diapir (Strozyk et al., 2012).

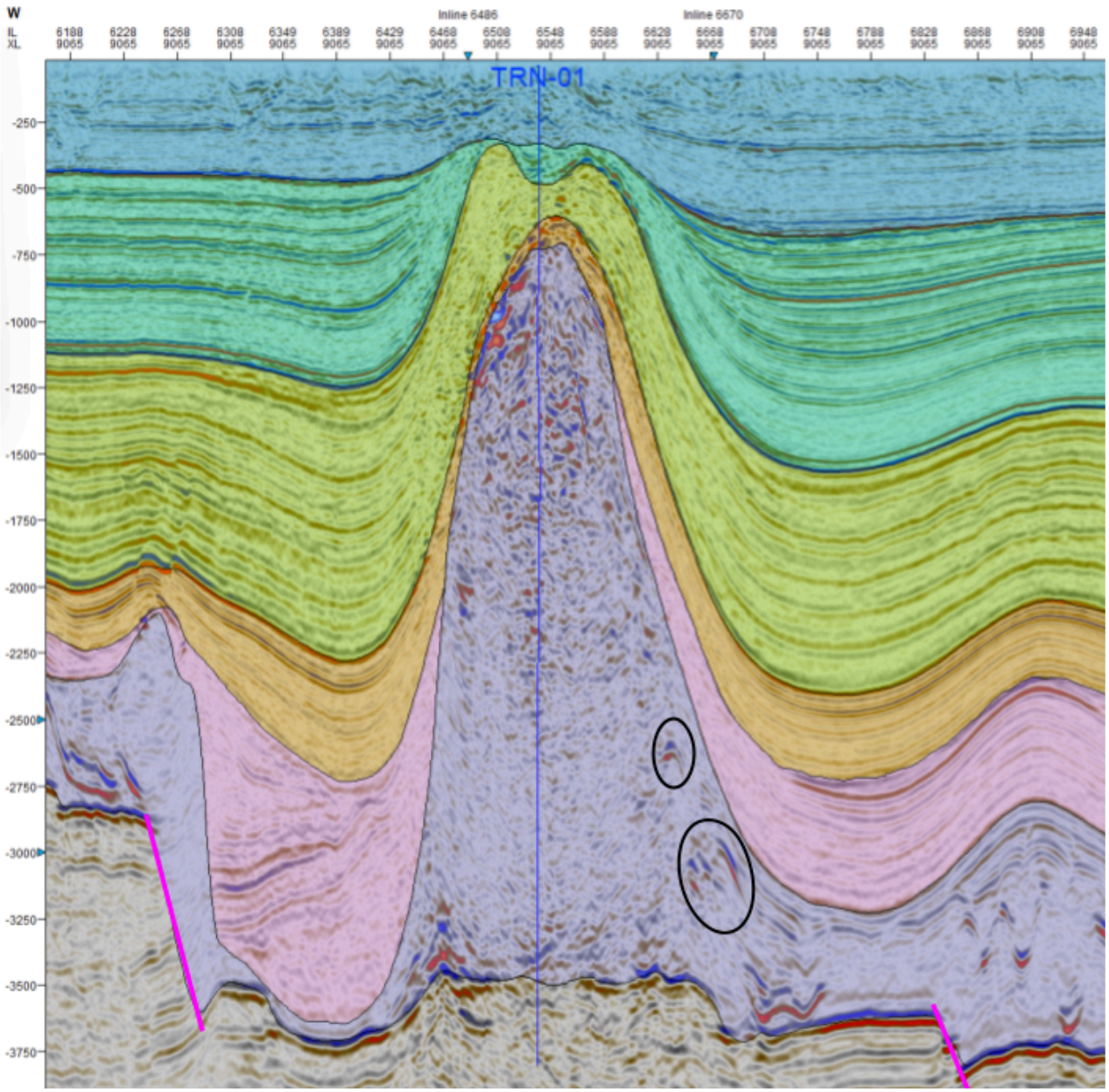

Figure 5a: W-E seismic section (X-line 9065) of the Ternaard diapir in Petrel. This section consists of the Zechstein Group (Purple), Lower and Upper Germanic Triassic Group (Pink), Rijnland Group (Orange), Chalk Group (Green), the Lower and Middle North Sea Group (Turquoise) and Upper North Sea Group (Blue). The well TNR-01 is indicated as a vertical blue line, examples of anhydrite banks (drifters) are delineated by a black circle, and some NW-SE trending faults (Bright pink).

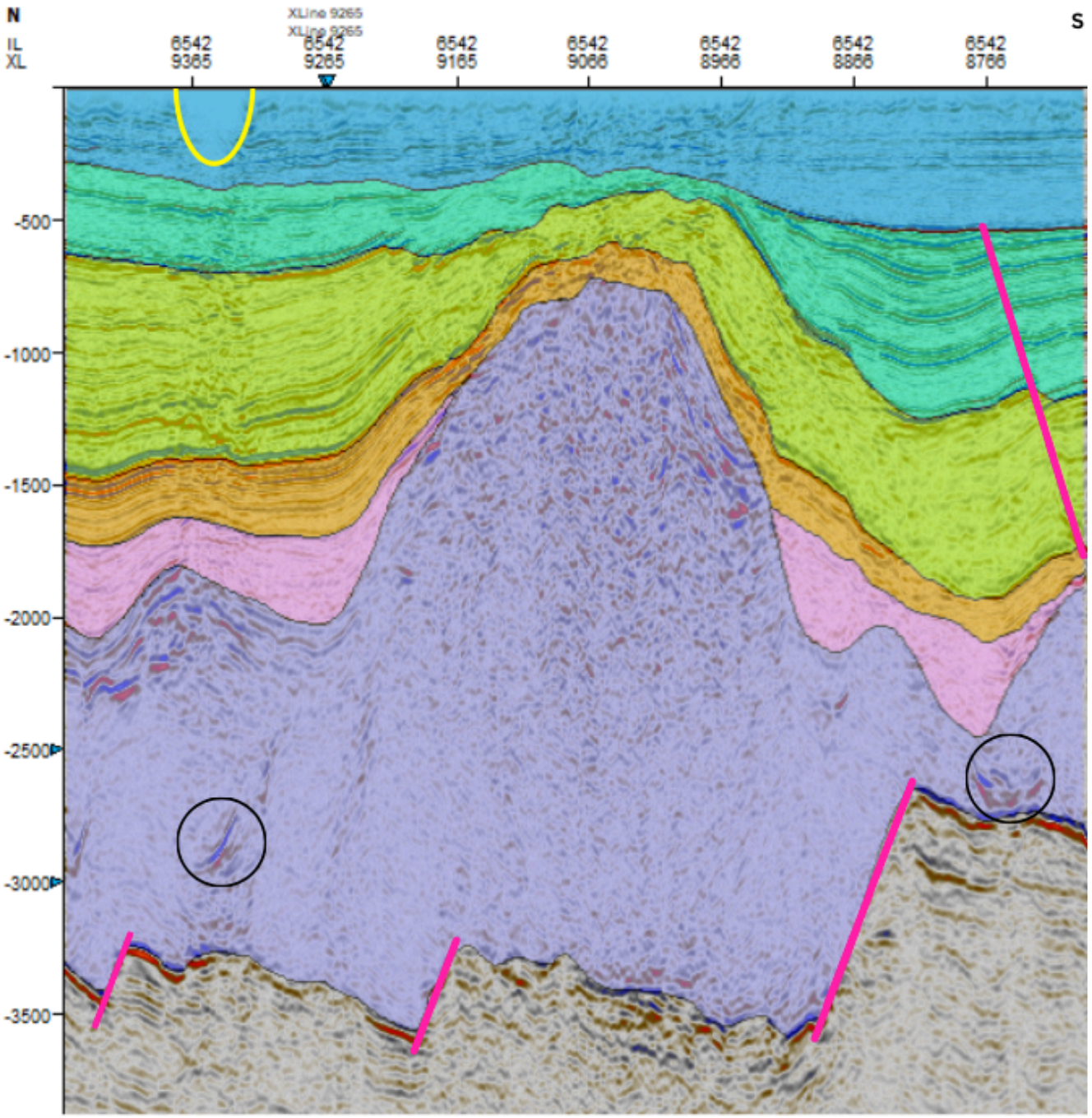

Figure 5b: N-S seismic section (In-line 6542) of the Ternaard diapir in Petrel. This section consists of the Zechstein Group (Purple), Lower and Upper Germanic Triassic Group (Pink), Rijnland Group (Orange), Chalk Group (Green), the Lower and Middle North Sea Group (Turquoise) and Upper North Sea Group (Blue). Examples of anhydrite banks (drifters) are delineated by a black circle, some NW-SE trending faults with opposite dipping orientations (Bright pink). A glacial channel is delineated in bright yellow.

Overlying units record the diapir's kinematic history, starting with the deposition of the Rotliegend Group following the formation of the Southern Permian Basin (TNO, 2014; Wong et al., 2007). The initiation of salit mobilisation is recorded in the Lower Germanic Triassic Group, where differential loading during early rifting events caused the salt to move from its source layer. This initial "pillow phase" continued into the Upper Germanic Triassic Group, where early uplift and crestal truncation associated with the Hardegesen Phase are visible as

weak, discontinuous reflectors (Table 2; Geluk, 2007). By the Triassic to Lower Cretaceous, the stratigraphic lakers showcase a significant truncation and thinning at the contact with the diapir, which indicates active piercement. Particularly, the Early Cretaceous Rijnland Group appears as a weak-to-medium amplitude, semi-transparent reflector that is frequently truncated at the crest, implying continued piercement and potential exposure during the Late Kimmerian phase (Jackson & Hudec, 2017; Pharaoh et al., 2010). In opposition, the Chalk Group is identified by a stratified, continuous, high-amplitude negative reflector, showcasing lateral continuity with gentle draping and minor crestal thinning. This suggests a period of regional stability during the Late Cretaceous (Almalki, 2023; Wong et al., 2007). The Cenozoic record indicates a shift in tectonic activity. Indeed, the Lower and Middle North Sea Groups are represented by stratified, medium-to-high amplitude negative reflectors showcasing pronounced crestal thinning and clear onlap terminations directly above the diapir, representing an interval of stratigraphic modification and high subrosion (Auzemery et al., 2025; Li et al., 2024). Finally, the Upper North Sea Group covers the entire structure as a strong, continuous positive reflector with clear onlap/downlap terminations. This uniform layer indicates that the diapir was finally contained and major salt movement had stabilized by the late Cenozoic (Almalki, 2023; TNO, 2014).

Table 2: Seismic reflectors of each stratigraphic group's base, their specific characteristics and geological importance.

Stratigraphic group base	**Reflector example**	**Reflector Characteristics**	**Geological Importance**
Base Upper North Sea Group	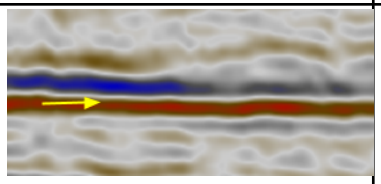	Strong, continuous positive reflector with clear onlap/downlap terminations.	**Post-Pyrenean phase and Cenozoic Loading:** final burial and containment of the diapir.
Base Middle and Lower North Sea Groups	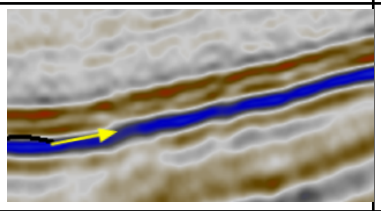	Stratified, medium-to-high amplitude, negative reflector.	**Pyrenean/Early Laramide Phases:** Period of stratigraphic modification and high subrosion.
Base Chalk Group	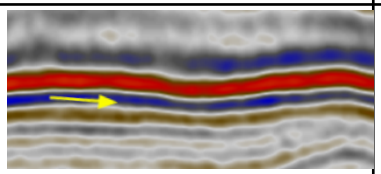	Stratified and continuous, high amplitude negative reflector.	**Sub-Hercynian Phase (Late Cretaceous):** Regional thermal subsidence and tectonic stability.
Base Rijnland Group	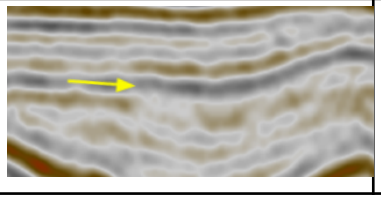	Weak to medium amplitude (strong over Zechstein, weaker over Triassic).	**Late Kimmerian phase (Late Jurassic - Early Cretaceous):** Base Cretaceous Unconformity (BCU), and main syn-rift phase (active diapiric piercement).

Base Upper Germanic Triassic Group	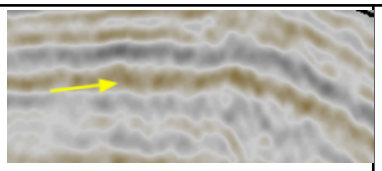	Weak, discontinuous reflector; low-amplitude.	**Hardegsen Phase (Early Triassic):** Early uplift and crestal truncation.
Base Lower Germanic Triassic Group	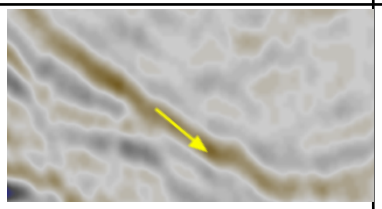	Medium-to-weak but becomes very strong when in direct contact with salt.	**Early Triassic Rifting:** Initiation of salt tectonics and initial salt mobilization.
Base Zechstein Group	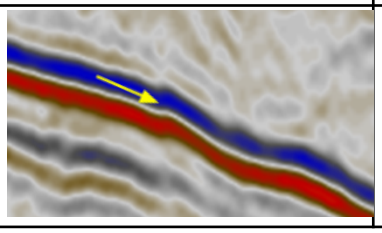	Very strong negative reflector; highly faulted with chaotic/transparent internal facies.	**Pre-salt structure and late Permian Transgression:** Deposition of the salt layer and control by pre-existing Variscan basement faults.

NW-SE trending normal faults (Fig. 5a & 5b) offset the post-salt stratigraphic layers, likely due to halokinetic stress and differential compaction. This could have led to enhanced localized subrosion, as those faults act as conduits for groundwater during earlier diapir activity (Appelo & Postma, 2005). Thickness maps (Appendix, Fig. A-C) showcase the spatial distribution of salt withdrawal. The most important withdrawal basin is associated with the Middle and Lower North Sea Groups (MLNSG), which form a concentric depocenter around the diapir (Fig. 5a & 5b). As mentioned previously, this stratigraphic layer shows extreme thinning and clear onlap terminations directly against the diapir compared to other stratigraphic groups. This geometry signifies a period of stratigraphic modifications and high subrosion linked to the mid-Cenozoic Pyrenean and Early Laramide tectonic phases (Table 2; Ten Veen et al., 2012). This intense salt withdrawal is supported by the regional truncation of the Lower North Sea Group at the Base Oligocene level. Ultimately, the seismic interpretation supports a diapiric evolution that can be divided in three stages: (1) a period of active piercement during the Jurassic-Early Cretaceous, characterized by rapid salt rise and the truncation of stratigraphic groups such as the Rijnland Group; (2) a period of passive diapirism and peak dissolution from the Late-Cretaceous to the mid-Cenozoic, defined by a relatively stable deposition of the Chalk Group followed by maximum salt withdrawal and subrosion during the MLNSG interval where internal salt flow may have been influenced by anhydrite banks (Strozyk et al., 2012; Ten Veen et al., 2012); and (3) a stage of burial from the late Cenozoic to the present, during which the diapir stabilized under the uniform Upper North Sea Group (Auzemery et al., 2025).

4.2 Salt budget

To quantify the seismic interpretation results, the salt budget was calculated for three specific stratigraphic layers, which are the youngest ones in order of sediment deposition: the Upper North Sea group, the Middle and Lower North Sea Groups and the Chalk group. As described in the methodology section, the domal and withdrawal areas of all 3 stratigraphic groups were delineated on thickness maps, as seen in the Appendix (Figs. A-C). In addition, a

table detailing the steps and values used for the salt budget calculation is also included in that same Appendix (Table A).

The youngest interval, the Upper North Sea Group (UNSG), records the lowest rate (Fig. 6) at ~5.98 m Myr^{-1} (~ 0.00598 mm yr^{-1}). Dissolution increased markedly during the deposition of the Middle and Lower North Sea Groups, reaching a maximum rate of ~27.19 m Myr^{-1} (~ 0.0272 mm yr^{-1}). This period represents the phase of most substantial halite loss. In the oldest evaluated interval, the Chalk Group, the rate decreases to an intermediate value of ~6.93 m Myr^{-1} (~ 0.00693 mm yr^{-1}), situating it between the pronounced MLNSG maximum and the lower UNSG rate. This progression suggests a pulse of intensified dissolution in the mid-Cenozoic, followed by a significant decline in subrosion activity towards the present day.

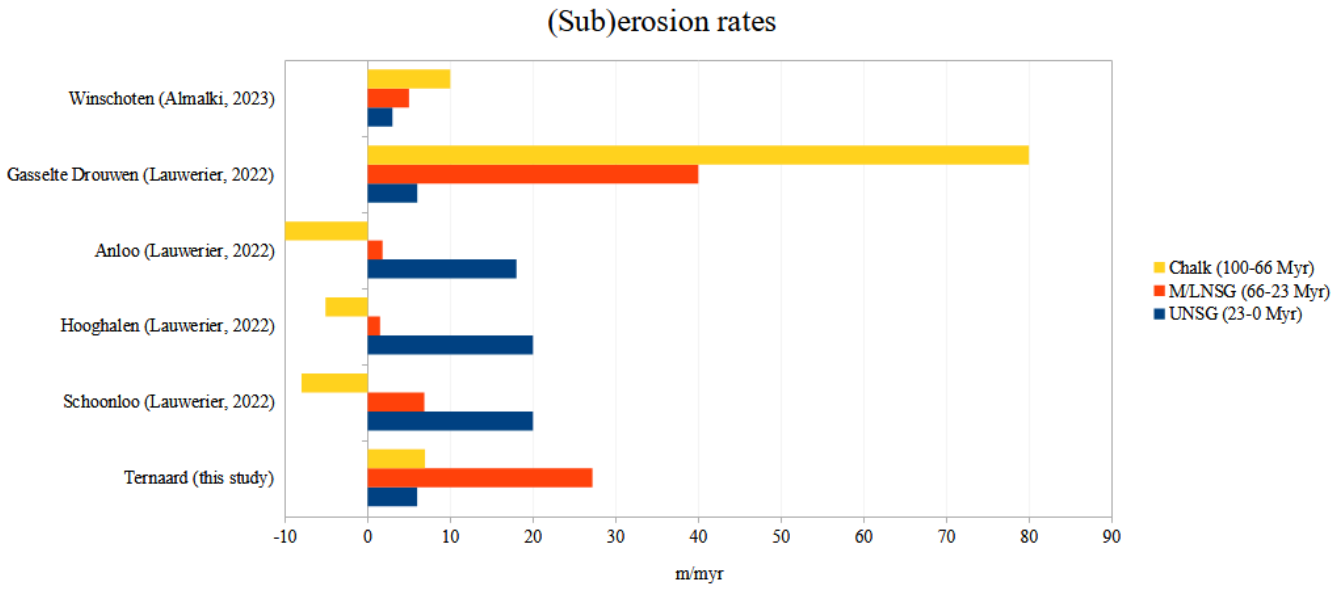

Figure 6: Subrosion rates (in m Myr^{-1}) per stratigraphic time interval per diapir

4.2.1 Sensitivity analysis of the salt budget

As many uncertainties are linked to the salt budget analysis, due to the time depth conversion and processing of the seismic data (Lauwerier et al., 2022), a salt budget sensitivity analysis was performed (Fig. 7). The results from this analysis clearly showcases that the calculated subrosion rates for the Ternaard diapir are consistently sensitive to variations (ranging from +/- 10% to +/- 20%) in both withdrawal-basin area (A_s) and domal-area (A_d), with changes in A_s generally producing a stronger response than equivalent changes in A_d. Ultimately, these results indicate that while the Ternaard subrosion values are quantitatively sensitive to the geometric assumptions and the relative ordering of intervals (MLNSG > Chalk Group > UNSG) dissolution-rates-wise remained stable across all tested scenarios.

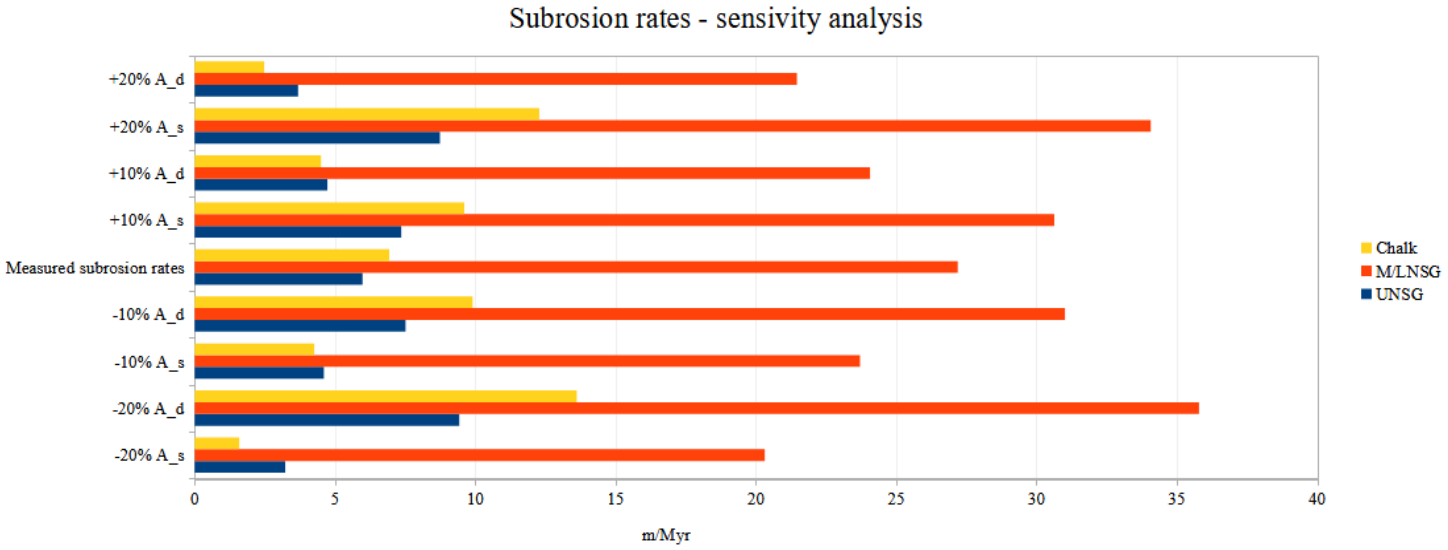

Figure 7: Sensitivity of calculated subrosion rates (in m Myr^{-1}) for the Ternaard diapir to ±10–20% variations in the withdrawal-basin area (A_s) and domal-area estimates (A_d). Bars show the resulting subrosion rates for the Chalk Group, MLNSG and UNSG intervals. The MLNSG interval displays the largest sensitivity to area adjustments, whereas the UNSG values remain comparatively stable across all scenarios.

4.3 0D modelling subrosion rates

The PHREEQC modelling results are presented in two parts: first, the influence of salinity on halite dissolution rate under open (no caprock) conditions is analysed across four Darcy fluxes (see section 4.3.2); second, the impact of caprock presence on subrosion is evaluated by comparing scenarios with caprock porosities of 1% and 10% (see section 4.3.2).

4.3.1 Influence of Salinity and Darcy flux on Halite dissolution rate

In total, 12 geochemical calculations were performed under the no-caprock regime, testing three distinct fluid salinities (1, 9, and 90 g L^{-1}) under four Darcy flux regimes ($1 * 10^{-6}$, $5 * 10^{-5}$, $5 * 10^{-4}$, and $5 * 10^{-3}$ m yr^{-1}). All simulations were performed over a reaction time of 1 year, with dissolution tracked kinetically and subrosion rates expressed in millimetres per year (mm yr^{-1}). Dissolution was tracked based on a unit surface area ($1\ m^2$) to determine the vertical retreat of the salt independent of total diapir size. The results are summarized in Table 3, which reports the calculated subrosion rates for each salinity–flux combination. Subrosion rates ranged from 0.12 mm yr^{-1} under the lowest flux ($1 * 10^{-6}$) and highest salinity (90 g L^{-1}), to 829.45 mm yr^{-1} under the highest flux ($5 * 10^{-3}$ m yr^{-1}) and lowest salinity (1 g L^{-1}).

Table 3: Halite dissolution rates (mm yr⁻¹) in function of Darcy fluxes and different reacting fluid compositions (ranging from 1 to 90 g L⁻¹ in salinity). This relationship is examined here for simulations without a caprock, where fluid–salt interaction is unconstrained by secondary mineral buffering.

Halite Subrosion rate [mm yr⁻¹]					
Darcy flux (m yr⁻¹)		$q = 1 * 10^{-6}$	$q = 5 * 10^{-5}$	$q = 5 * 10^{-4}$	$q = 5 * 10^{-3}$
Groundwater inflow fluid salinity (g L⁻¹)	1	0.17	8.30	82.95	829.45
	9	0.16	5.10	77.90	805.42
	90	0.12	2.94	53.30	589.96

Darcy flux exerted the strongest control on subrosion rates across all salinity conditions. For a given salinity, subrosion rates increased linearly with increasing flux over several orders of magnitude. For example, under 1 g L⁻¹ salinity, rates rose from 0.17 mm yr⁻¹ (at $q = 1 * 10^{-6}\, m/yr$) to 829.45 mm yr⁻¹ (at $q = 5 * 10^{-3} m/yr$), which is an increase of three orders of magnitude. This linear response reflects the advection-limited nature of dissolution in the 0D system, where higher flux delivers more undersaturated fluid per unit time.

Salinity also significantly influenced subrosion, though its effect was secondary to Darcy flux. Lower-salinity fluids (1 and 9 g L⁻¹) produced consistently higher dissolution rates than the high-salinity brine (90 g L⁻¹). At the highest flux ($5 * 10^{-3} m/yr$), subrosion decreased from 829.45 mm yr⁻¹ (1 g L⁻¹) to 589.96 mm yr⁻¹ (90 g L⁻¹), a reduction of approximately 29%. At lower fluxes, the relative impact of salinity was more pronounced; at $q = 1 * 10^{-6}\, m/yr$, the rate dropped by 35% between 1 g L⁻¹ and 90 g L⁻¹. This trend reflects the stronger chemical undersaturation (more negative saturation index) results in increased dissolution. Ultimately, the results demonstrate a coupling between hydrodynamic and geochemical controls: high Darcy flux amplifies the geochemical advantage of low-salinity fluids; indeed, the most rapid subrosion occurs under high-flux and low-salinity conditions.

4.3.2 Effect of caprock thickness on halite dissolution rates

In total, 16 geochemical simulations were performed under the caprock regime, testing two distinct caprock thicknesses (13 and 65 m), with two porosities (1 and 10%), four Darcy fluxes ($1 * 10^{-6}$, $5 * 10^{-5}$, $5 * 10^{-4}$, and $5 * 10^{-3}$ m yr⁻¹), and under the fluid salinity with the highest dissolution potential (1 g L⁻¹). All simulations were performed over a reaction time of 1 year, with dissolution tracked kinetically and subrosion rates expressed in centimetres per million years (cm Myr⁻¹). A tortuosity factor of 3 was chosen for all runs, to represent the complex, non-linear pore geometries found in highly compacted evaporite

caprocks (Appelo & Postma, 2005; Auzemery et al., 2025). The results are summarized in Table 4.

Table 4: *Halite dissolution rates (cm myr⁻¹) in function of Darcy fluxes, caprock thickness and porosity. All the simulations were performed using the lowest salinity (1 g L⁻¹) groundwater inflow composition, a caprock thickness of both 13 and 65 meters, a caprock porosity of 1 and 10%, as well as a fixed caprock tortuosity factor of 3.0.*

Halite Subrosion rate [cm Myr⁻¹]									
Darcy flux (m yr⁻¹)		$q = 1 * 10^{-6}$		$q = 5 * 10^{-5}$		$q = 5 * 10^{-4}$		$q = 5 * 10^{-3}$	
Caprock thickness		13 m	65 m	13 m	65 m	13 m	65 m	13 m	65 m
Caprock porosity	1%	10.409	6.1359	44.753	9.1529	45.895	9.1995	46.01	9.2041
	10%	10.543	10.541	352.13	87.06	447.61	91.534	458.95	91.995

Those simulations indicate that the subrosion rates are very sensitive to caprock properties at high Darcy fluxes ($q \geq 5 * 10^{-5} m\,yr^{-1}$). At the highest tested Darcy flux ($q = 5 * 10^{-3} m\,yr^{-1}$) and 10% porosity, increasing the caprock thickness from 13 to 65 m results in a five-fold reduction in halite dissolution, going from 458.95 cm Myr⁻¹ (~ 0.0046 mm yr⁻¹) to 91.99 cm Myr⁻¹ (~ 0.00092 mm yr⁻¹). Under the same hydraulic conditions, a decrease in porosity from 10% to 1% further suppresses the rate to ~ 9.20 cm Myr⁻¹ for the 65m caprock thickness.

The subrosion rates follow a slightly different trend at the lowest Darcy flux tested ($q = 1 * 10^{-6} m\,yr^{-1}$). At this flow rate, the thickness of the caprock does not appear to play a significant role on the subrosion rates. For the 10% porosity scenario, the subrosion rate is essentially identical (10.54 cm Myr⁻¹), whether the caprock has a thickness of 13 or 65 meters. In the 1% porosity scenario, the difference between the 13m thickness (10.40 cm Myr⁻¹) and the 65m thickness (6.13 cm Myr⁻¹) is still much lower than at higher fluxes.

Additionally, the results for the 65m caprock thickness showcase some kind of plateau effect. Indeed, as the Darcy flux increases by two orders of magnitude (from $q = 5 * 10^{-5}$ to $q = 5 * 10^{-3} m\,yr^{-1}$), the subrosion rate for the 1% porosity caprock remains very similar, increasing only by a small margin, from 9.15 to 9.20 cm Myr⁻¹. Ultimately, all those simulations showcase that the halite dissolution rate increases with decreasing caprock thickness, increasing porosity and Darcy flux (Fig. 8).

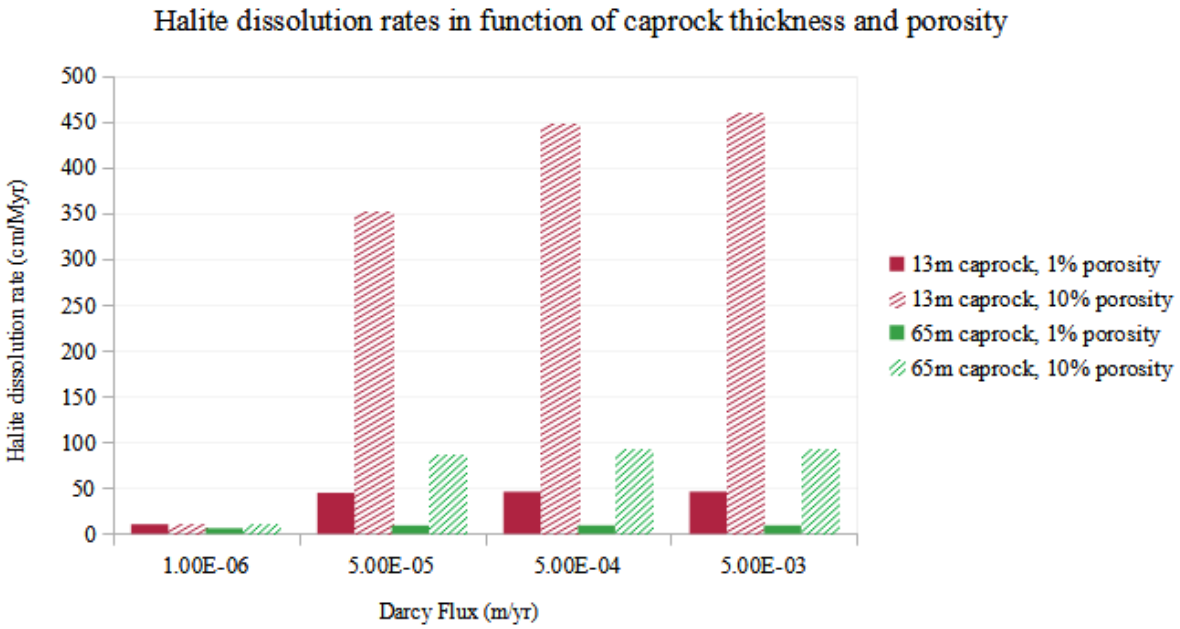

Figure 8: Sensitivity of halite subrosion rates to caprock thickness and matrix porosity across varying hydraulic regimes. The bar chart illustrates the transition from a flow-controlled regime at low Darcy flux ($q = 1 * 10^{-6} m\,yr^{-1}$) to a transport-limited regime at higher fluxes ($q = 5 * 10^{-3} m\,yr^{-1}$). The Ternaard site thickness (~13 m) shows a heightened sensitivity to porosity increases compared to the hypothetical 65 m scenario. All simulations used a fixed tortuosity factor of 3.0 and a baseline groundwater inflow fluid salinity of 1 g L^{-1}.

5. DISCUSSION

5.1 Integrating seismic interpretation and salt budget for Ternaard

Ternaard's modern geometry and conservative salt budget result from its position on the stable Friesland Platform, which dictated its response to North Sea geodynamics (Pharaoh et al., 2010; Verweij, 2003). While Zechstein structures mobilized during Triassic extension (Stewart et al., 2007), Ternaard avoided the intense compression and rapid uplift characteristic of the inverting Lower Saxony or Central Grabens (Van Wijhe, 1987; Nalpas et al., 1995). This tectonic sheltering is showcased by both the asymmetric geometry of the elongated, tilted diapir and the somewhat uniform thickness of the Chalk Group over the structure, which acts as a protective regional seal. This sealing effect prevented early exposure to aggressive fluid systems that drove extreme subrosion in other diapirs (De Jager, 2007). Because of that, Ternaard's subrosion rates are lower than reference diapirs like Gasselte-Drouwen (Fi.g. 6), which were subject to both more aggressive vertical piercement and long-lived, burial-induced fluid flow from compactional dewatering of thick basinal deposits (Li et al., 2024; Strozyk et al., 2012).

The fluids responsible for this interaction could have been sourced from different regimes. During active piercement phases in the Mesozoic, compaction-driven fluids expelled from adjacent basinal sediments could have circulated along the diapir flanks (Verweij, 2003). The initiation of the salt piercement was likely localized by the Hantum Fault Zone (Fig. 1). Indeed, this provided a zone of crustal weakness, triggering a transition from a salt pillow to a growing diapir (Verweij, 2003), primarily along the steeper N-E flank, where the crest of the diapir reached its shallowest point of 615 m. In its current shallow setting, the dominant fluid source is topography-induced meteoric water from Pleistocene-to-recent sea-level minimums. As noted by Li et al. (2024), this fresh water supply encourages aggressive subrosion and dictates the geochemical environment for secondary mineral formation at the salt interface. The presence of NW-SE trending faults (Fig. 5a & 5b), which are likely features related to the Hantum Fault zone or halokinetic stress, can further increase dissolution by acting as high-permeability conduits for groundwater. Nevertheless, the seismic interpretation confirms that the Chalk Group maintains a more uniform thickness over the structure compared to diapirs in inverted basins. This is direct evidence of Ternaard's position on the tectonically stable Friesland Platform, which experienced muted inversion during the Subhercynian phase, allowing for the preservation of that seal (De Jager, 2007; Verweij, 2003).

This particular evolution persisted into the Cenozoic. Diapirs were predominantly shaped by deep burial-induced processes, including differential loading and compaction-driven fluid flow systems (Verweij, 2003; Japsen, 1999). Ternaard’s evolution, however, was punctuated by a distinct Mid-Cenozoic phase of erosion associated with the Pyrenean uplift of the Southern Early Tertiary High, evidenced by pronounced truncation of the Lower North Sea Group, specifically at the Base Oligocene level, where regional tilting led to the removal of significant Eocene sections (Wong et al., 2007; Ten Veen et al., 2012). The geometric asymmetry observed in the seismic profiles (Fig. 5) highlights the non-uniform salt withdrawal into the withdrawal basins during these phases. Additionally, the limited burial depth beneath the Waddenzee places the diapir’s crest within an active coastal hydrodynamic regime. This proximity to near-surface water circulation helps the ongoing physical and chemical modification of the salt-caprock interface.

Ultimately, Ternaard’s modern configuration, characterized by a preserved Chalk seal, moderate Neogene truncation, and a seismically chaotic crest suggestive of active shallow processes, is the signature of a diapir that evolved on a stable structural high influenced by basement faulting. Its history was punctuated by specific regional tectonic events, rather than sustained basinal tectonics, with its present-day morphology being actively modified by shallow, topography-driven hydrological processes. This tectono-geographic context ultimately explains its distinctive profile when compared to diapirs in more basinal settings (Li et al., 2024).

5.2 0D modelling subrosion rates

5.2.1 Controls on Halite dissolution: from advection to diffusion

The 0D PHREEQC simulations reveal a shift in the processes governing salt loss depending on the presence of a caprock. In the no-caprock scenarios, subrosion is primarily advection-limited. The linear relationship between Darcy flux and dissolution rate suggests that the system is largely limited by the rate at which undersaturated water is delivered to the salt interface (Li et al., 2024). As the driver of fluid renewal, the flux determines the volume of undersaturated water available, subrosion rates increase linearly from 0.17 mm yr^{-1} ($at\ q = 1 * 10^{-6} m/yr$) to a peak of 829.45 mm yr^{-1} ($at\ q = 5 * 10^{-3} m/yr$). While groundwater inflow fluid salinity acts as a secondary control, its impact is significant: increasing salinity from 1 g/L to 90 g/L reduces the dissolution rate by approximately 29% to 35% depending on the flux, as the fluid approaches thermodynamic saturation (SI = 0). However, as highlighted by Auzemery et al. (2025), the peak rates of ~830 mm yr^{-1} observed in these no-caprock scenarios are considered an unphysical overestimation for long-term safety assessments. While these tests replicate the kinetic potential of unprotected salt, they are geologically unsustainable. Auzemery et al. (2025) notes that implementing realistic caprock lithologies and brine density effects reduces subrosion to "possibly only a few meters per million years." Thus, the 0D results confirm that neglecting insoluble protective barriers leads to subrosion estimates that do not align with the geological record.

5.2.2 The protective effect of the caprock

The presence of a caprock transforms the subrosion regime from kinetic-dominated dissolution to diffusion-limited stability. As shown in Table 5, even a thin 13 m caprock provides a "protective efficiency" of 99.99% (at 1% porosity), reducing the vertical retreat from 829.45 mm yr^{-1} to just 0.46 m Myr^{-1} (0.00046 mm yr^{-1}). This creates a hydraulic disconnect, putting the diapir in a state of transport-limited stability (Appelo & Postma, 2005; Auzemery et al., 2025). Indeed, the dissolution rate is no longer only a function of the groundwater velocity (q), but rather the ability of ions to migrate through the caprock's pore network via molecular diffusion (Jackson & Hudec, 2017; Sanford, 1992).

The modeling results highlight that the Ternaard diapir exists in a transitional state where the degree of protection is highly dependent on the hydraulic forcing. In the 65 m scenarios, a "diffusion plateau" is reached where subrosion remains fixed at approximately ~ 9.20 cm Myr^{-1} regardless of flow increases; here, the slow migration of Na^{+} and Cl^{-} through the caprock acts as a permanent bottleneck. In contrast, the 13 m caprock at Ternaard lacks the diffusive path length required to completely decouple the salt from aquifer dynamics. At 10% porosity, the subrosion rate climbs significantly with flux, reaching 458.95 cm Myr^{-1} (4.59 m Myr^{-1}). This suggests that the modern stability noted by Almalki (2023) and TNO (2014) is likely due to high caprock quality (low porosity and high tortuosity) rather than thickness alone. If the 13 m caprock were highly fractured (>10% porosity), the diapir would exhibit significantly more crestal deflation than the ~5.98 m Myr^{-1} recorded in the Upper North Sea Group. However, the risk associated with this thin caprock is mitigated by the regional

hydraulic regime. At the lowest tested Darcy flux ($q = 1 * 10^{-6} m\,yr^{-1}$), subrosion rates remain consistently low and show no significant sensitivity to changes in porosity or thickness. This indicates that as long as regional groundwater pressure gradients remain low, a smaller caprock thickness does not inherently increase the risk of rapid halite dissolution. Ultimately, even a 13 m layer provides a near-total hydraulic disconnect that protects the diapir from the aggressive, "unphysical" dissolution rates observed in open-salt systems (Auzemery et al., 2025).

Table 5: Protective efficiency of the Caprock seal, based on the most aggressive scenario ($q = 5 * 10^{-3} m\,yr^{-1}$, and 1 g L^{-1} groundwater inflow fluid salinity).

	Subrosion rate (m Myr^{-1})	Rate reduction (%)
No caprock (diapir exposed)	829,000	/
13 m caprock, 1% porosity	0.46	**99.99 % or greater**
13 m caprock, 10% porosity	4.59	
65 m caprock, 1% porosity	0.09	
65 m caprock, 10% porosity	0.92	

5.4 Synthesis: Integrating the 0D geochemical results with past subrosion rates

The no-caprock simulations performed in this study replicate the magnitude of the peak results found in Li et al. (2024), confirming that the geochemical engine accurately captures a maximum kinetic potential of up to ~830,000 m Myr^{-1}; however, as argued by Auzemery et al. (2025), such rates are geologically "unphysical" because they neglect brine density stratification and the rapid formation of protective insoluble residues. The seismic interpretation supports this, identifying a mid-Cenozoic "dissolution pulse" during the Middle and Lower North Sea Group (MLNSG) of only 27.19 m Myr^{-1}. This seismic rate is significantly higher than the modeled rates for a thick, low-porosity caprock (<100 cm Myr^{-1}.) but remains orders of magnitude lower than exposed-salt scenarios, suggesting that during this period of active diapiric rise, the caprock was likely thinner or fractured, temporarily increasing its effective porosity to levels exceeding the 13 m / 10% porosity scenario (4.59 m Myr^{-1}; Jackson & Hudec, 2017).

As the system stabilized during the Upper North Sea Group (UNSG) deposition, subrosion dropped to 5.98 m Myr^{-1}, a value that aligns closely with the modeled results for a 13 m caprock with low-to-moderate porosity. This transition indicates that Ternaard has moved from an active, fractured state into its current state of relative tectonic dormancy (Almalki, 2023; Auzemery et al., 2025). Compared to the deeper, more heavily capped diapirs described by Auzemery et al. (2025), Ternaard remains in a transitional state; while it has escaped the

aggressive dissolution potential described by Li et al. (2024), the thin caprock still retains enough hydraulic sensitivity to allow for meters-per-million-year subrosion.

In the future, the potential evolution of the diapir remains speculative but is likely governed by two competing feedbacks: continued subrosion may lead to the further accumulation of insoluble anhydrite and clay, potentially thickening the caprock and driving the system toward the highly stable, plateaued rates seen in the 65 m scenarios (~ 9.20 cm Myr^{-1}). However, any renewed tectonic activity or significant changes in the regional hydraulic gradient could increase the Darcy flux (q) or induce crestal fracturing (Ten Veen et al., 2012), which, given Ternaard's current thickness (~13 m), would lead to a more pronounced increase in dissolution compared to thicker-capped structures.

6. CONCLUSIONS

The long-term integrity of rock salt as a host medium for radioactive waste disposal depends fundamentally on the stability of the salt barrier against subrosion. This study investigated the Ternaard diapir, a structure characterized by its shallow crest and unusually thin (~13 m) caprock, to determine if such a limited seal can provide the necessary isolation over geological timescales. By synthesizing seismic salt budget analysis with 0D reactive transport modeling in PHREEQC, this study quantified the subrosion rates of the past 100 million years and projected the diapir's stability into the future.

Analysis of the diapir's morphological evolution confirms that its position on the tectonically stable Friesland Platform was the primary control on its long-term preservation. Seismic evidence, including a preserved Chalk Group "shell" and a chaotic crestal facies, indicates that Ternaard exhibited a more passive diapiric evolution, avoiding the rapid vertical piercement and subsequent erosional loss that affected salt structures within the Lower Saxony Basin. Salt budget calculations support this, revealing a subrosion history defined by moderate pulses rather than rapid, sustained destruction. The identified mid-Cenozoic "dissolution pulse" of 27.19 m Myr^{-1} (2,719 cm Myr^{-1}) during MLNSG deposition likely represents a period of active diapiric rise that temporarily fractured the developing caprock. However, as tectonic forcing decreased during the Upper North Sea Group (UNSG) deposition, subrosion dropped to 5.98 m Myr^{-1} (598 cm Myr^{-1}), marking a transition toward the diapir's modern state of structural isolation.

Geochemical modeling investigated the "no-caprock" potential versus the current "caprock-protected" reality of the Ternaard diapir. For an exposed, "no-caprock" scenario, subrosion rates are governed by Darcy flux and salinity, reaching a maximum of ~830,000 m Myr^{-1}, a value confirmed as "unphysical" for long-term safety assessments but useful for benchmarking the reactive capacity of the system (Li et al., 2024; Auzemery et al., 2025). The implementation of the specific 13 m caprock thickness identified at Ternaard shifts the system

into a transport-limited regime, providing a "protective efficiency" of 99.99% at 1% porosity. Even under high Darcy flux conditions ($q = 5 * 10^{-3} m\, yr^{-1}$), this thin caprock decreases subrosion to just 0.46 m Myr^{-1} (46 cm Myr^{-1}).

Ultimately, the study concludes that Ternaard exists in a transitional state of transport-limited stability. While the 13 m caprock acts as a near-total hydraulic disconnect under current low-energy groundwater conditions, its limited thickness makes the diapir more sensitive to future changes in Darcy flux or matrix porosity than structures with thicker caprocks (e.g., 65 m caprock scenarios). However, given the current state of tectonic dormancy and the observed efficiency of the existing seal, the Ternaard diapir exhibits a high degree of stability relative to salt-volume loss. Assuming no significant mechanical breaching of the caprock matrix, the subrosion rates are expected to remain within the range of a few centimeters to meters per million years. This low rate of vertical retreat suggests that the Zechstein salt at Ternaard can maintain its structural integrity and remain a viable, isolated geological unit over a 1 Ma timeframe.

7. RECOMMENDATIONS

To improve the strength of geochemical simulations, future work should extend the current 0D modelling into a 1D model by coupling the PHREEQC framework with a reactive-transport solver. This integration is necessary to accurately simulate the coupled processes of fluid advection, solute dispersion, and chemical reaction, which would provide stronger constraints on both the timing and spatial distribution of dissolution events. Furthermore, a comparative analysis between the transitional Ternaard diapir and the nearby Pieterburn diapir is recommended. Although both are located in the onshore-coastal (or near-coastal) domain, Pieterburen features a significantly thicker caprock (~90 m), providing an ideal baseline to isolate how caprock thickness, rather than just geographic location, governs long-term subrosion patterns. Such an investigation would clarify how varying caprock geometries and hydraulic conditions influence diapir evolution across the Netherlands. Additionally, incorporating dynamic feedbacks, such as the progressive accumulation of insoluble residues to thicken the caprock over time, would further refine the predictive accuracy of long-term salt barrier integrity.

8. REFERENCES

Almalki, B. (2023). *Zechstein salt structures evolution in the northeastern Netherlands* [Internship Report]. Utrecht University & COVRA N.V.

Appelo, C.A.J. & Postma, D. (2005). *Geochemistry, Groundwater and Pollution (2nd Ed.)*. CRC Press/Balkema, Leiden, The Netherlands.

Auvray, C., Matenco, L., & Bartol, J. (2023). *Hydrological connectivity and salt dissolution in the Dutch subsurface.* [Technical Report Summary].

Auzemery, A., Matenco, L., Beekman, F., & Bartol, J. (2025). *Tectonic and hydrodynamic drivers of salt subrosion in the North Sea Basin.* [Technical Report Summary].

COVRA. N.V. (2024). *COPERA SALT 2024: A conditional safety case and feasibility study for the Geological Disposal of Radioactive Waste in Rock Salt in the Netherlands*. (Compiled by Bartol, J., et al.). COVRA. N.V.

De Jager, J. (2007). Geological development. In Th.E. Wong, D.A.J. Batjes, & J. de Jager (Eds.), *Geology of the Netherlands* (pp. 5–26). Royal Netherlands Academy of Arts and Sciences.

Doornenbal, J. C., & Stevenson, A. G. (Eds.). (2010). *Petroleum Geological Atlas of the Southern Permian Basin Area.* EAGE Publications b.v.

Duin, E.J.T. & Doornenbal, J.C. & Rijkers, R.H.B. & Verbeek, J.W. & Wong, Theo. (2006). Subsurface structure of the Netherlands - Results of recent onshore and offshore mapping. Netherlands J. Geosci.. 85. 10.1017/S0016774600023064.

García-Monzón, G., Bartol, J., & Matenco, L. (2022). *Caprock variability and spatial differences in subrosion intensity in Dutch Zechstein diapirs.* [Project Data].

Gast, J., Dusar, M., Breitkreuz, C., Gaupp, R., Schneider, J. W., Stemmerik, L., & Geluk, M. C. (2010). Rotliegend. In J. C. Doornenbal & A. G. Stevenson (Eds.), *Petroleum Geological Atlas of the Southern Permian Basin Area* (pp. 101–121). EAGE Publications b.v.

Geluk, M. C. (2007). Permian. In Th.E. Wong, D.A.J. Batjes, & J. de Jager (Eds.), *Geology of the Netherlands* (pp. 63–106). Royal Netherlands Academy of Arts and Sciences.

Gent, H. V., Urai, J. L., & Keijzer, M. de. (2011). The internal geometry of salt structures – A first look using 3D seismic data from the Zechstein of the Netherlands. *Journal of Structural Geology*, *33*(3), 292–311. https://doi.org/10.1016/j.jsg.2010.07.005

GeoExpro. (2021). *The Ternaard discovery: A complex fault-block play in the Wadden Sea.* GeoExpro Magazine, 18(3).

Griffioen, J., van der Grift, B., & Broers, H. P. (2016). *Geochemistry of groundwater in the Netherlands: Chemical compositions of Dutch deep aquifers and reservoirs.* TNO-Report.

Jackson, M. P. A., & Hudec, M. R. (2017). *Salt Tectonics: Principles and Practice*. Cambridge: Cambridge University Press.

Japsen, P. (1999). Overpressured Cenozoic shale mapped from velocity anomalies relative to a base line for marine shale, North Sea. Petroleum Geoscience 5, 321-336.

Lauwerier, W. (2022). *Evolution of the Zechstein salt diapirs in the north-eastern Netherlands* [Internship Report]. Utrecht University & COVRA N.V.

Li, M., Collard, N., Schueller, S., Matenco, L., Nader, F. H., Beekman, F., Cacas, M.-C., & Bartol, J. (2024). *Quantitative modelling of diapirism and geochemical evolution of the subrosion process of salt domes in the northeast Netherlands for radioactive waste disposal (Project Report*. Utrecht University & IFP Energies Nouvelles.

Nalpas, T. Le Douaran, S., Brun, J.-P., Unternehr, P. and Richert, J.-P. 1995. Inversion of the Broad Fourteens Basin (offshore Netherlands), a small-scale model investigation. Sedimentary Geology 95, 237-250.

NLOG. (2023). *Geological data of the Netherlands: Friesland Platform and Wadden Sea sectors.* Netherlands Oil and Gas Portal.

Parkhurst, D.L., & Appelo, C.A.J. (2013). *Description of input and examples for PHREEQC version 3—A computer program for speciation, batch-reaction, one-dimensional transport, and inverse geochemical calculations*. U.S. Geological Survey Techniques and Methods, book 6, chap. A43.

Peryt, T. M., Geluk, M. C., Mathiesen, A., Schmidt, S. T., & Kockel, F. (2010). Zechstein. In J. C. Doornenbal & A. G. Stevenson (Eds.), *Petroleum Geological Atlas of the Southern Permian Basin Area* (pp. 123–147). EAGE Publications b.v.

Pharaoh, T. C., Dusar, M., Geluk, M. C., Kockel, F., Poprawa, P., & Steinmetz, T. (2010). Tectonic evolution. In J. C. Doornenbal & A. G. Stevenson (Eds.), *Petroleum Geological Atlas of the Southern Permian Basin Area* (pp. 25–57). EAGE Publications b.v.

Rijkers, R. H., & Duin, E. J. (1994). *National Hydrological Instrument (NHI) and REGIS II: Structural and hydrodynamic models of the Dutch subsurface.* TNO-NITG.

Sanford, W. E. (1992). Ground-water flow and salt transport in the vicinity of salt domes. *Journal of Hydrology*, 129(1-4), 373–384.

Seni, S. J., & Jackson, M. P. A., 1983. Evolution of salt structures, East Texas diapir province, Part 2: Patterns and rates of halokinesis. AAPG bulletin, 67(8), 1245-1274.

Stewart, S. A., Ruffell, A. H., & Harvey, M. J. (2007). *Relationship between Triassic rifting and early salt mobilization in the Southern North Sea.* Geological Society, London, Special Publications.

Strozyk, F., van Gent, H. W., Urai, J. L., & Kukla, P. A. (2012). 3D seismic study of complex salt structures and internal layers in the Zechstein Group, NE Netherlands. *Netherlands Journal of Geosciences*, 91(3), 307–325.

Ten Veen, J. H., van Gessel, S. F., & den Dulk, M. (2012). Dynamics of salt-filled fault zones and their influence on the development of the Southern North Sea Basin. *Marine and Petroleum Geology*, 35(1), 205–219.

TNO - Geological Survey of the Netherlands. (2014). *Informatieblad Zoutpijler Ternaard: Technisch-geologisch overzicht.* (Factsheet No. 2014.11.07). https://www.nlog.nl

Van den Haute, P., & Vercoutere, C. (1990). *Middle Jurassic regional doming and erosion on the Friesland Platform: A fission-track study*.

Van Wijhe, D.H. 1987a. The structural evolution of the Broad Fourteens Basin. In: Brooks, J. and Glennie, K. (eds). Petroleum Geology of North West Europe. Graham and Trotman, 315-323

Verweij, J. M. (2003). *Fluid flow systems analysis on geological timescales in onshore and offshore Netherlands* [Doctoral Thesis,]. Vrije Universiteit Amsterdam.

Weert, Annelotte & Camanni, Giovanni & Mercuri, Marco & Ogata, Kei & Vinci, Francesco & Tavani, Stefano. (2025). Displacement analysis of basin-scale reactivated normal faults: Insights from the West Netherlands Basin. Journal of Structural Geology. 192. 105356. 10.1016/j.jsg.2025.105356.

Wong, T. E., Batjes, D. A. J., & de Jager, J. (2007). *Geology of the Netherlands*. Royal Netherlands Academy of Arts and Sciences.

Zirngast, M. (1996). The development of the salt dome Gorleben (NW Germany) based on 3D seismic data. *Tectonophysics*, 265(1-2), 129–144.

9. APPENDIX

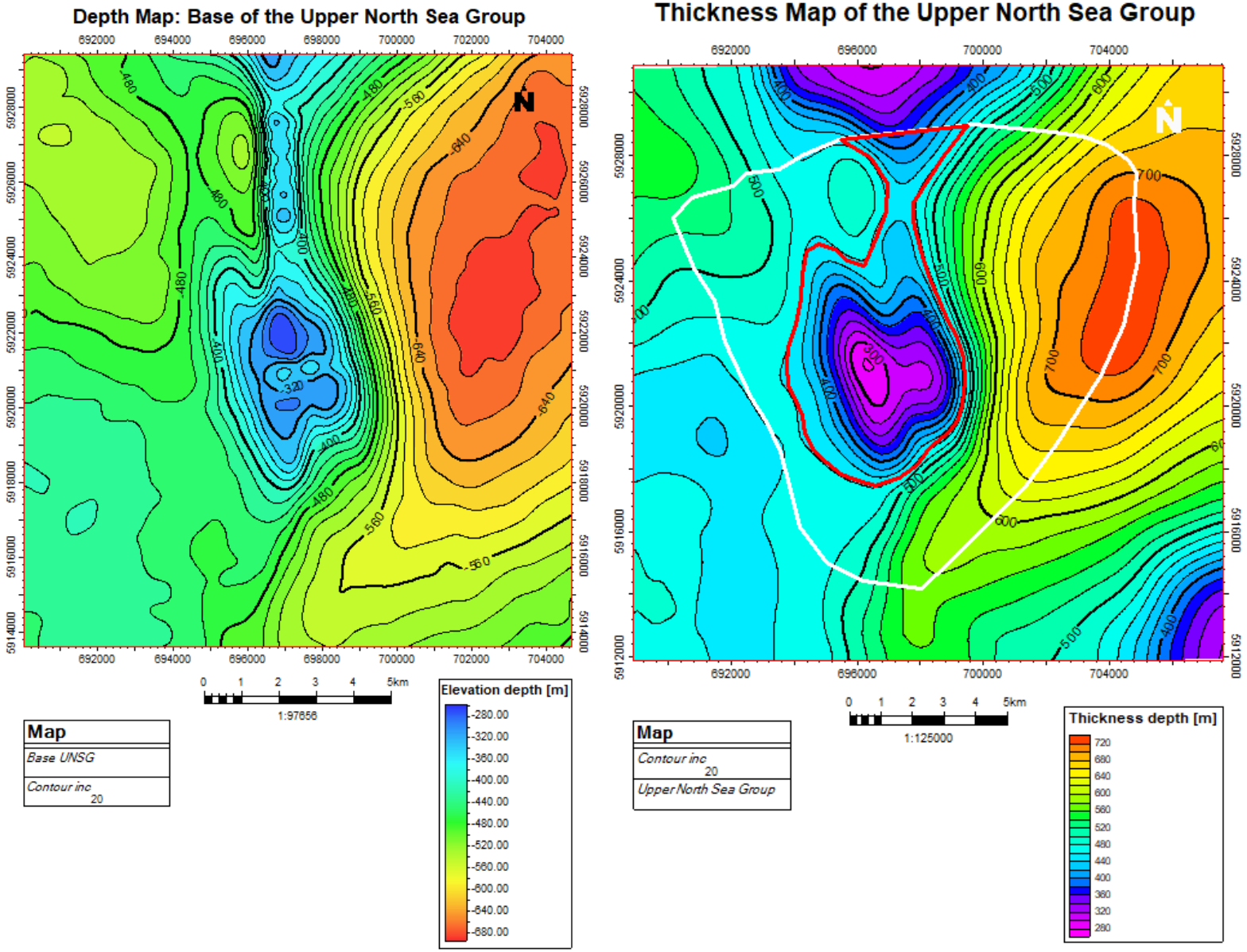

Figure A: Depth Map (left) of the Upper North Sea Group Base and thickness map (right) of the Upper North Sea Group, made in Petrel. The white polygon represents the withdrawal area, and the red one delineates the domal area.

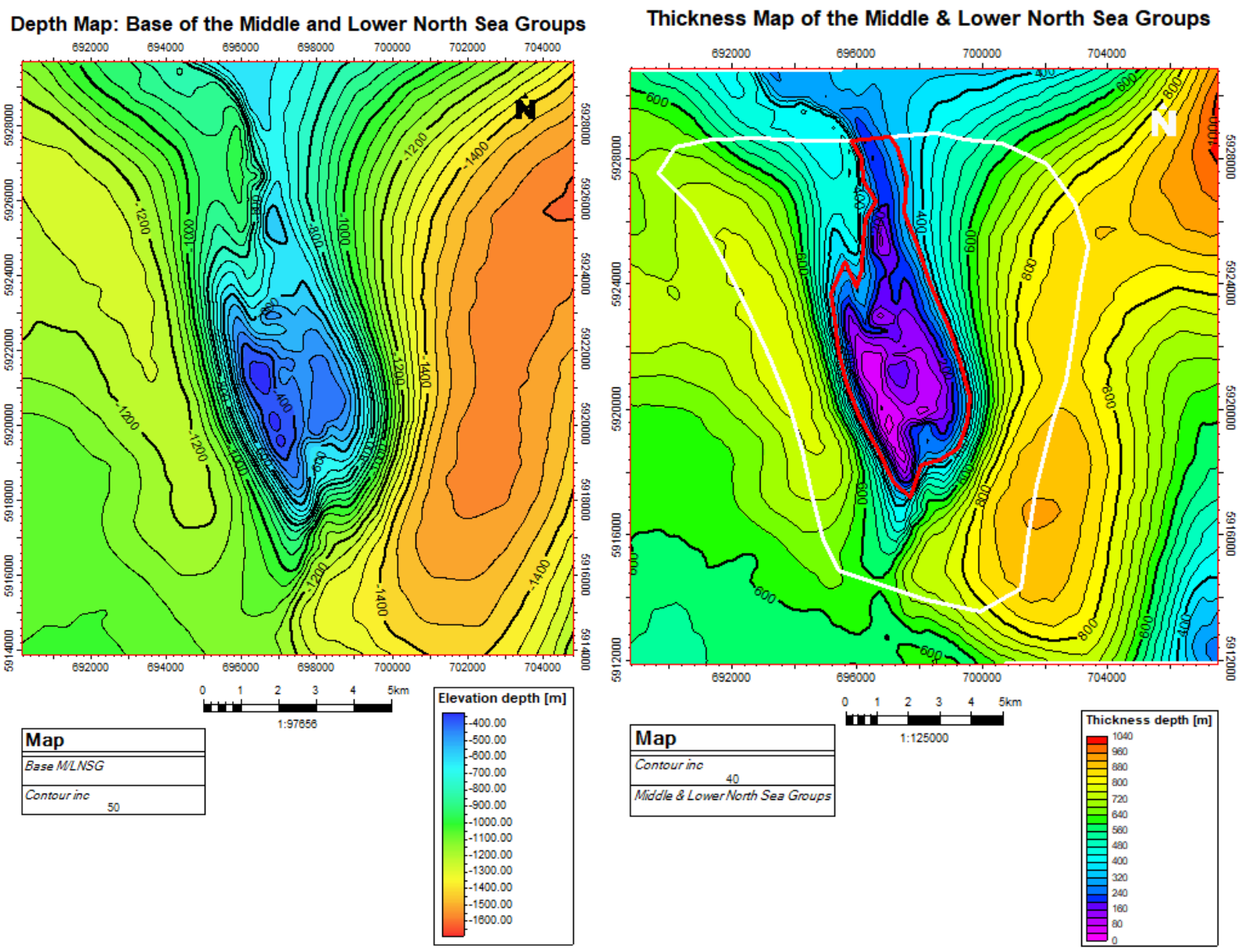

Figure B: Depth Map (left) of the Middle and Lower North Sea Groups Base and thickness map (right) of the Middle and Lower North Sea Groups, made in Petrel. The white polygon represents the withdrawal area, and the red one delineates the domal area.

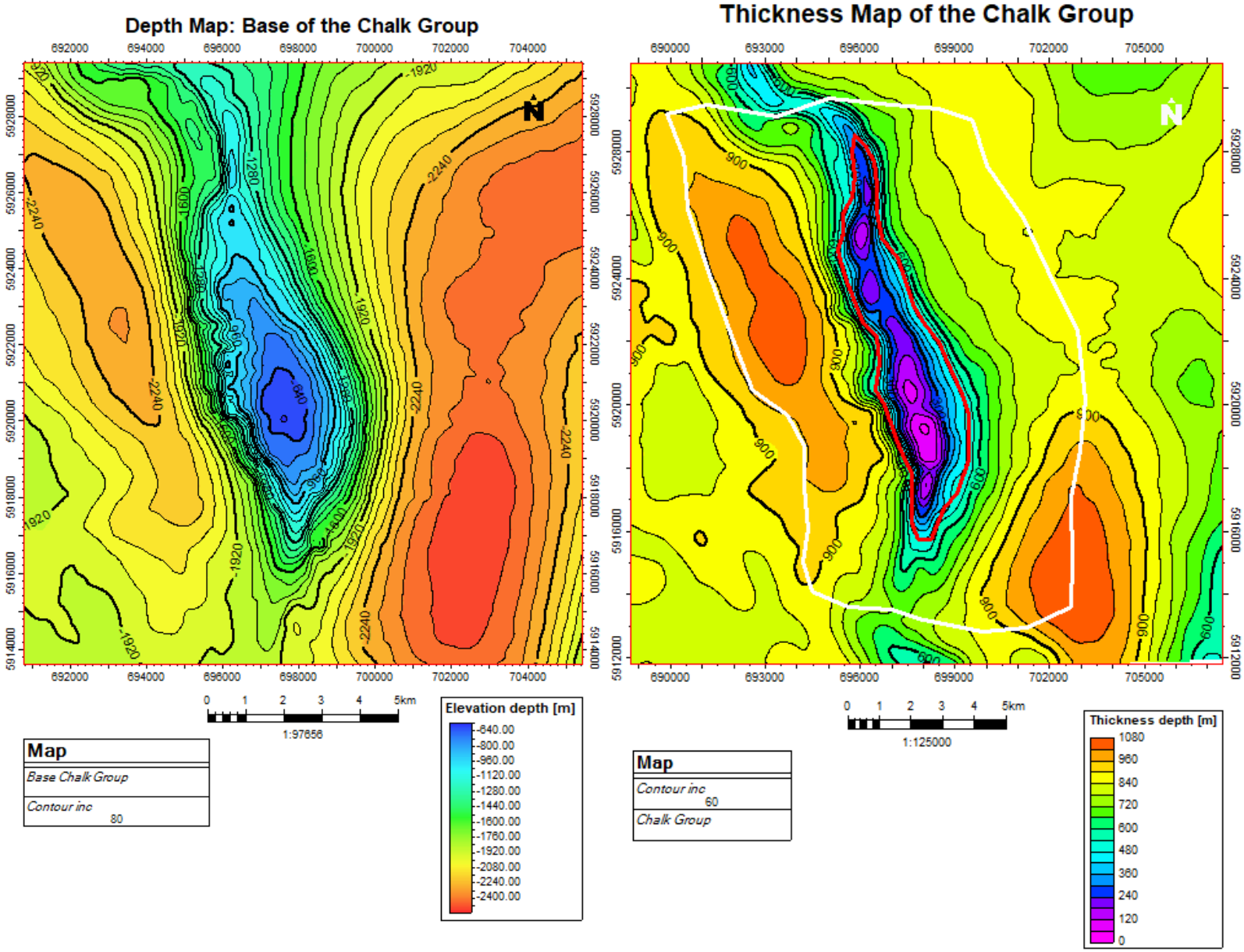

Figure C: Depth Map (left) of the Chalk Group Base and thickness map (right) of the Chalk Group, made in Petrel. The white polygon represents the withdrawal area, and the red one delineates the domal area.

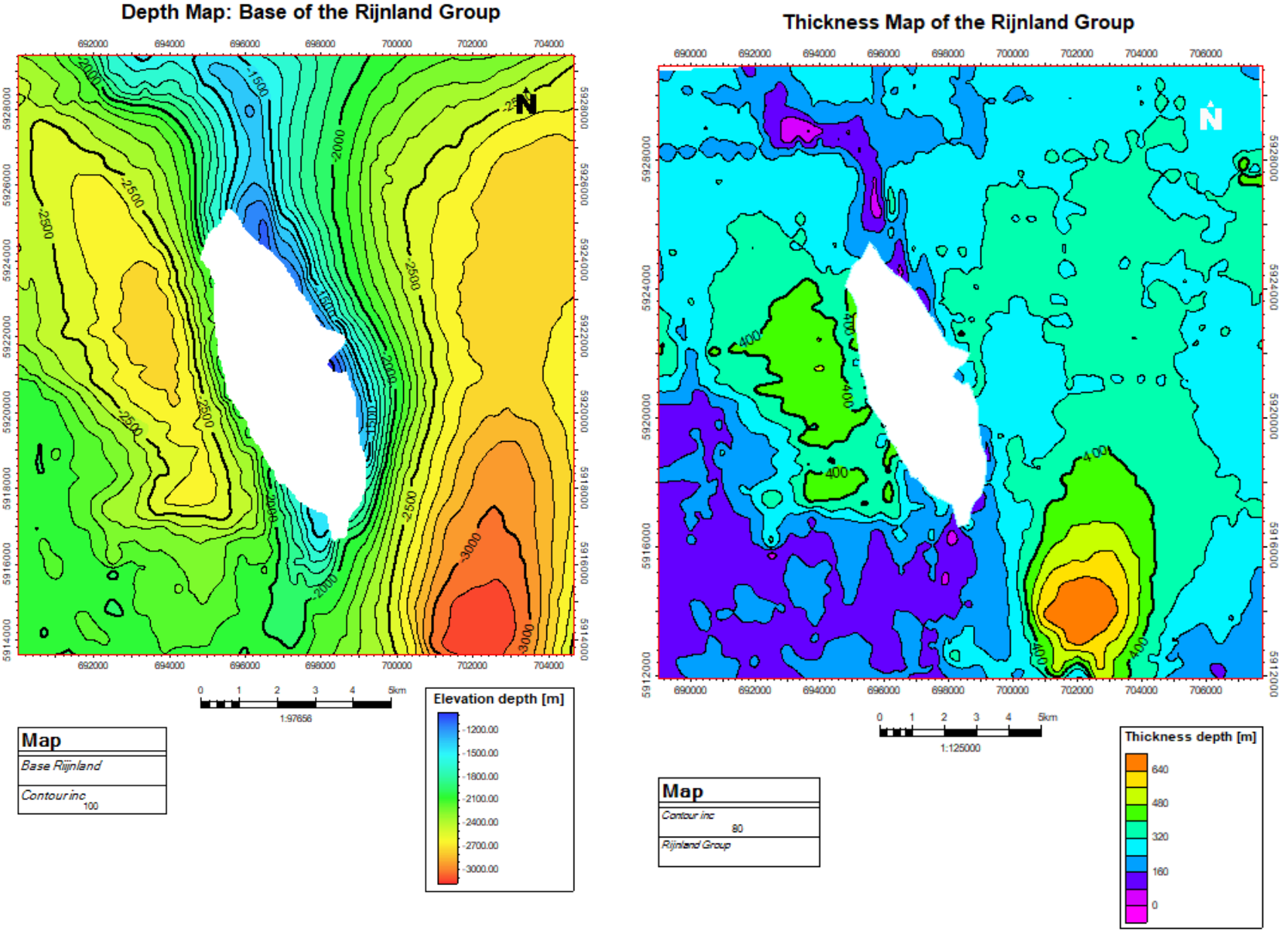

Figure D: Depth Map (left) of the Rijnland Group Base and thickness map (right) of the Rijnland Group, made in Petrel. The empty (white) areas represent areas where the stratigraphic group was truncated by other stratigraphic groups, such as the Zechtein salt.

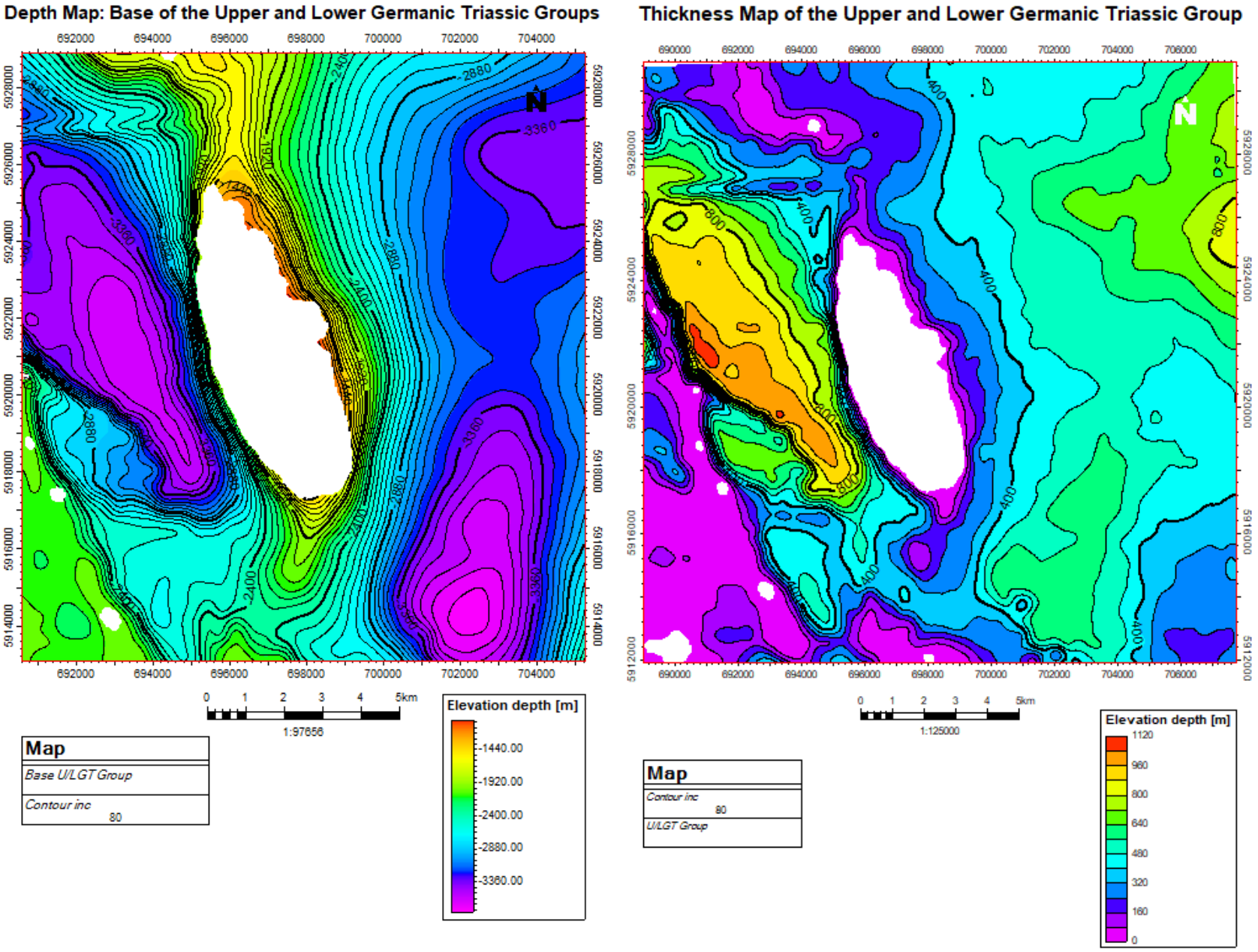

Figure E: Depth Map (left) of the Upper and Lower Germanic Triassic Groups Base and thickness map (right) of the Upper and Lower Germanic Triassic Groups, made in Petrel. The empty (white) areas represent areas where the stratigraphic group was truncated by other stratigraphic groups, such as the Zechtein salt.

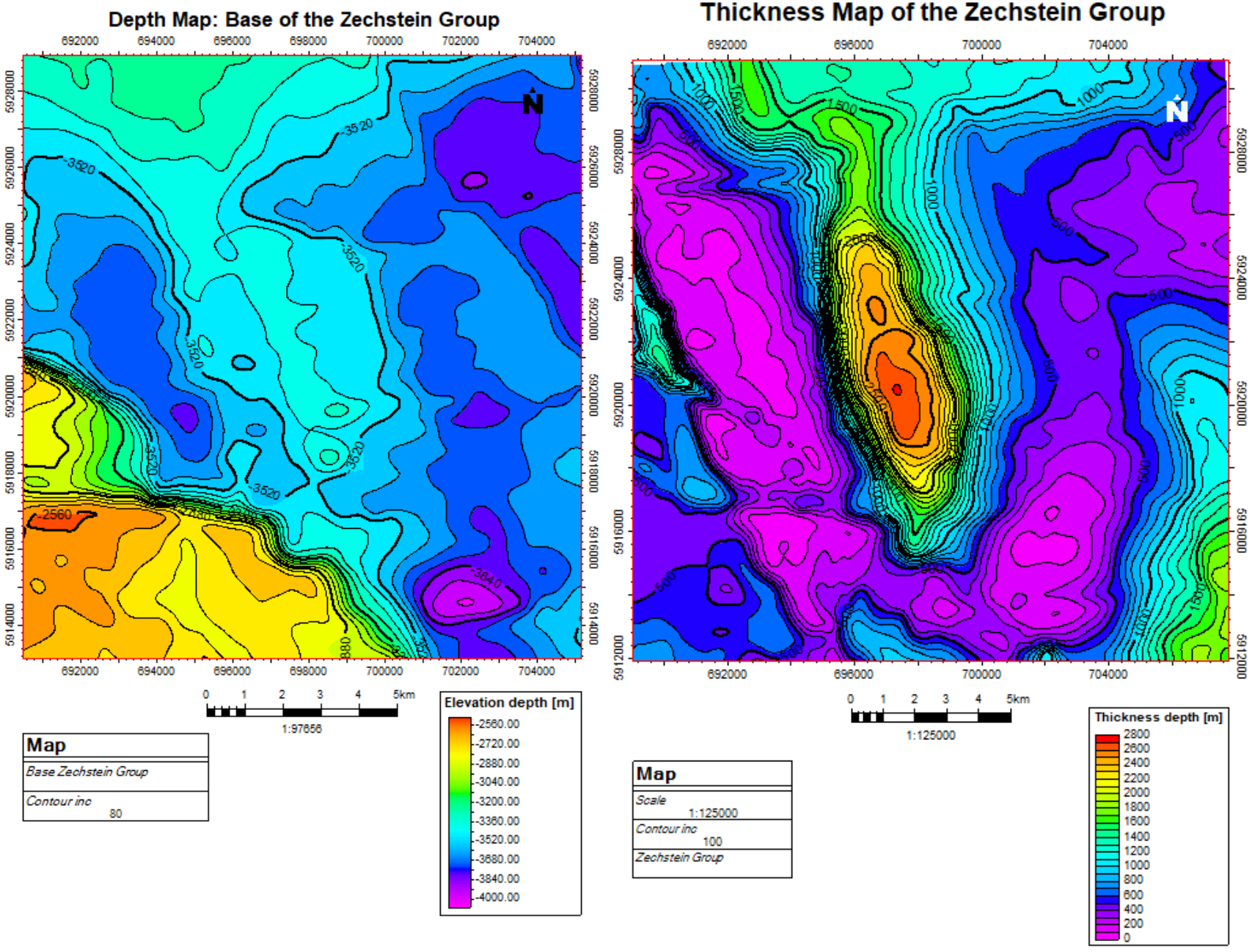

Figure F: Depth Map (left) of the Zechstein Group Base and thickness map (right) of the Zechstein Group, made in Petrel.

Units	Time (Ma)	LSB Thickness mean (m)	Salt diapir influence area (m^2)	Domal area (m^2)	Withdrawal basins areas (m^2)	Mean sediment thickness in withdrawal basins (m)	Sediment volume	Gross growth	Min Sediment thickness on top of the diapir	Net growth	Suberosion	Subrosion rate (m/Myr)	Subrosion rate (mm/yr)
Notations and Calculations	Δt	h_n	A_i	A_d	A_s	h_{sw}	$V_{sed} = (h_{sw} - h_n) * A_s$	$H_{gross} = V_{sed} / A_d$	h_{top}	$H_{net} = h_n - h_{top}$	$H_{sub} = H_{gross} - H_{net}$	$R_{m/myr} = H_{sub} / \Delta t$	$R_{mm/yr} = R_{sub} * 0.001$
Upper North Sea Group	*23*	458	*1.46E+08*	*3.81E+07*	1.08E+08	570.45	1.21E+10	316.99	*278.62*	179.38	137.62	5.98	0.0059
Middle/Lower North Sea Group	43	320	*1.33E+0.8*	*2.47E+07*	1.08E+08	657.28	3.65E+10	1478.72	10.61	309.39	1169.33	27.19	0.027
Chalk Group	34	720	1.25E+08	1.95E+07	1.05E+08	889.52	1.77E+10	908.79	46.95	673.05	235.75	6.93	0.0069

Table A: Summary of input parameters and derived values for the salt budget analysis of the Ternaard diapir, following the volumetric method of Zirngast (1996). The table details the stratigraphic intervals and corresponding durations used to reconstruct the diapir's evolution over the last 100 million years.Column 3 gives the regional reference thickness. The values for the Middle/Lower North Sea Group were retrieved from Lauwerier et al. (2022) as they represented the average sediment thickness in the near Ternaard, but the Upper North Sea Group sediment thickness was estimated from regional averages (with the use of Dinolocket). Areas for the salt structure and surrounding withdrawal basins (Columns 4-6) were delineated from the thickness maps provided in Appendix A (Fig. B-D). The gross salt growth (Column 8) is calculated from the sediment volume displaced within the withdrawal basins. Net growth (Column 9) is determined by the difference between regional subsidence and the actual sediment thickness preserved above the diapir crest, as identified in seismic and well data. The resulting subrosion values (Column 10) represent the difference between gross and net growth. All vertical rates (m/Myr) are obtained by normalizing these volumetric changes over the absolute time spans defined in Column 2.Input file A: PHREEQC input script for the kinetic dissolution of Halite, testing with a Dacry flux $q = 1 * 10^{-6}$ *m/yr, and an inflow water composition of salinity 90 g/L. The run was performed using the Pitzer.dat thermodynamic database. This script was created based on Parkhurst & Appelo (2013). The output from this simulation is given below in Table B of this Appendix.*

```
TITLE 0D modelling, No caprock, q = 1e-6 m/yr, Salinity = 90 g/L

RATES
Halite_diss                                  # name of rate
-start
10 si_h = SI("Halite")                       # calculate Saturation index (SI) of Halite
20 IF (M <= 0) THEN moles = 0 : SAVE moles : END       # if no salt is left, stop reaction
30 k25 = 10^(-0.21)                 # Rate constant for Halite dissolution at 25 degrees Celsius (from Li et al., 2024)
40 ea = 7400                        # Activation energy (J/mol) for the Arrhenius equation (from Li et al., 2024)
50 rg = 8.314                       # Universal gas constant (J/mol*K)
60 tkel = TC + 273.15               # convert Celsius to Klevin
80 kt = k25 * EXP(-ea/rg * (1/tkel - 1/298.15))          # Temperature correction for the rate constant
90 ssa = PARM(1)                             # retrieve Reactive surface area from the KINETICS block (- parms)
100 sa = ssa * M * 58.44                     # calculate total surface area (m2) based on current moles
110 omega = 10^(si_h)                        # convert SI to Saturation ratio (IAP/Ksp)
120 driving = 1 - omega                      # calculate chemical driving force
130 IF (driving < 0) THEN driving = 0  # do not count precipitation
140 rate = kt * sa * driving                 #  compute dissolution rate (mol/s)
150 moles = rate * TIME                      # multiply rate by the duration of 1 timestep
160 SAVE moles                               # update the integration for the kinetic reactor
-end

SOLUTION 1 Groundwater Inflow_composition   # values from Griffioen et al., 2016 (used by Li et al., 2024)
    temp      30                        # in Celsius
    pH        6.4
    pe        12
    redox     pe
    units     mg/l
    density   1
    Alkalinity 231 as HCO3
    Ca        3958
    Cl        59130
    K         310
    Mg        920
    Na        30400
    S(6)      78.8 as SO4
    Si        102 as H4SiO4
    -water    1                         # mass of water (kg) reacting per year, changes with each Darcy flux

KINETICS 1
Halite_diss
    -formula  Cl 1 Na 1                          # chemical formula of the reactant
    -m        3660                               # Moles of Halite available (large reservoir)
    -m0       3660                                # Initial Halite moles
```

```
    -parms    0.0001                                  # Reactive Surface area, in m2/kg (from Li et al., 2024)
    -steps    31536000 in 1 steps                     # 1 Year in seconds

SELECTED_OUTPUT 1
    -file         subrosion_batch_results_1e-6_90.txt      # name of the output file
    -time         true                                      # include time in the output file
    -totals       Na  Cl                                    # track the Na and Cl concentrations
    -kinetic_reactants  Halite_diss                         # track how many moles of Halite were dissolved
    -user_punch   true                                      # enable the calculations written out below

USER_PUNCH
-headings Subrosion_mm_yr
10 moles_diss = KIN_DELTA("Halite_diss")          # retrieve moles during this timestep
20 molar_mass = 58.44                             # g/mol
30 density_salt = 2160                            # kg/m3
40 area = 1                                       # unit cross-flow area, m2
50 mass_kg = (moles_diss * molar_mass) / 1000     # convert moles to kg
60 vol_m3 = mass_kg / density_salt                # convert kg to volume (m3) using density
70 thickness_m = vol_m3 / area                    # calculate height of lost salt layer (m)
80 thickness_mm = thickness_m * 1000              # convert m to mm
90 PUNCH thickness_mm
END
```

Table B: Example of a PHREEQC simulation, testing with a Darcy flux $q = 1 * 10^{-6}$ m/yr, and an inflow water composition of salinity 90 g/L. This outlines the calculations the software is running, from the amount of Halite moles removed from the system after a simulation of 1 year.

EXAMPLE CALCULATIONS: Salinity 90 g/L, No Caprock			
Component	**Calculations**	**Value**	**Units**
Darcy Flux, q	/	0.000001	m/yr
Bulk surface area, A_{bulk}	/	1000	m^2
Timestep, Δt	/	1	yr
Water Volume, V_w	$V_w = q * A_{bulk} * \Delta t$	0.001	m^3
Water mass, WM	$WM = V_w * 1000$	1	kg
Porosity, ϕ	/	0.01	/
Flow velocity, υ	$\upsilon = q / \Phi$	0.0001	m/yr

Moles dissolved, Δ_n	Result from Phreeqc run	**4.3873**	mol
Molar Mass Halite, M_{Hal}	/	0.05844	kg/mol
Halite density, ρ_{Hal}	/	2160	kg/m^3
Halite volume lost, V_{lost}	$V_{lost} = (\Delta_n * M_{Hal}) / \rho_{Hal}$	0.0001187	m^3
Subrosion rate, $R_{m/yr}$	$R_{m/yr} = V_{lost} / (S_{cell} * \Delta t)$	1.1870E-04	m/yr
Subrosion rate, $R_{mm/yr}$	$R_{m/Myr} = R_{m/yr} * 1,000$	0.1187	mm/yr

```
TITLE 0D modelling, 13 m caprock, q = 1e-6 m/yr, Salinity 1 g/L, caprock porosity 1%

RATES
Halite_Caprock                                          # name of rate
-start
 10  L = 13                                             # caprock thickness
 20  phi = 0.01                                         # caprock porosity
 30  D_eff = 1.6e-9 * (phi / 3.0)                       # effective diffusion
 50  RSA = 1e-4                                         # m2/kg
 60  Area_geom = 1000                                   # Geometric area of diapir (m2)
 70  Thickness_active = 1                               # 1 m active salt layer (focus at interface)
 80  Mass_active = Area_geom * Thickness_active * 2160  # kg of salt
 90  Surface_area = RSA * Mass_active                   # Reactive surface Area (m2)
 100 C_sat = 6.1                                        # value from the Pitzer.dat database
 110 C_now = TOT("Cl")                                  # current amount of Cl
 130 Flux = (D_eff / L) * (C_sat - C_now) * 1000        # Applies Fick's first law (mol/m2/s)
 150 rate = Flux * Surface_area                         # converts flux into total dissolution rate (mol/s)
 160 moles = rate * TIME                                # total moles dissolved
 170 SAVE moles
-end

SOLUTION 1 Groundwater Inflow_solution      # values from Griffioen et al., 2016 (used by Li et al., 2024)
    temp      30              # in Celsius
    pH        7.7
    units     mg/l
    -water    1               # mass of water (kg) reacting per year, changes with each Darcy flux (Table. C)
    Alkalinity 458 as HCO3
    Ca        46.5
    Cl        460
    Na        582
    K         25
    Mg        19.8
    S(6)      43.2 as SO4
```

```
SAVE Solution 1
END

USE Solution 1

EQUILIBRIUM_PHASES 1                    # Caprock minerals seeking equilibrium (moles available in excess)
    Anhydrite 0 10
    Calcite   0 10
    Gypsum    0 10
    Dolomite  0 10

KINETICS 1
Halite_Caprock                          # name of rate previously defined
    -formula  Cl  1 Na  1               # chemical formula of the reactant
    -m        3600000                   # Moles of Halite available (large reservoir)
    -m0       3600000                   # Initial Halite moles
    -parms    0.0001                    # Reactive Surface area, in m2/kg (from Li et al., 2024)
    -tol      1e-12
-steps       31536000 in 1 steps        # length of simulation (in seconds, 1 year)
-step_divide 1
-runge_kutta 6                          # high-order numerical integration method to ensure accuracy
-bad_step_max 500

SELECTED_OUTPUT 1
    -file         subrosion_cap_results_1e-6_13_1.txt        #name of the output file
    -time         true                  # include time in the output file
    -totals       Na  Cl                # track the Na and Cl concentrations
    -kinetic_reactants  Halite_Caprock  # track how many moles of Halite were dissolved
    -user_punch   true                  # enable the calculations written out below

USER_PUNCH
-headings mm_yr m_Myr cm_Myr
10 moles_diss = KIN_DELTA("Halite_Caprock")     # retrieve moles during this timestep
20 mass_kg = (moles_diss * 58.44) / 1000        # moles to kg
30 vol_m3 = mass_kg / 2160                      # convert kg to volume (m3) using density
40 area = 1000                                  # diapir surface area (m2)
50 rate_m_yr = vol_m3 / area                    # get the dissolution rate in m/yr
60 rate_mm_yr = rate_m_yr * 1000                # convert rate in mm/yr
70 rate_m_Myr = rate_m_yr * 1e6                 # convert rate in m/Myr
80 rate_cm_Myr = rate_m_yr * 100 * 1e6          # convert rate in cm/Myr
90 PUNCH rate_mm_yr, rate_m_Myr, rate_cm_Myr
END
```

Input file B: PHREEQC input script for the kinetic dissolution of Halite, testing with a Dacry flux $q = 1 * 10^{-6}$ *m/yr, caprock thickness of 13 m and 1% salinity, and an inflow water composition of salinity 1 g/L. The run was performed using the Pitzer.dat thermodynamic database. This script was created based on Parkhurst & Appelo (2013). The output from this simulation is given below in Table C of this Appendix.*

EXAMPLE CALCULATIONS: Salinity 90 g/L, 13 m, 1% porosity caprock, Q = 1e-6 m/yr			
Component	**Calculations**	**Value**	**Units**
Darcy Flux, q	/	0.000001	m/yr
Bulk surface area, A_{bulk}	/	1000	m^2
Timestep, Δt	/	1	yr
Water Volume, V_w	$V_w = q * A_{bulk} * \Delta t$	0.001	m^3
Water mass, WM	$WM = V_w * 1000$	1	kg
Porosity, ϕ	/	0.01	/
Moles dissolved, Δ_n	Result from Phreeqc run	**2.2679**	mol
Molar Mass Halite, M_{Hal}	/	0.05844	kg/mol
Halite density, ρ_{Hal}	/	2160	kg/m^3
Halite volume lost, V_{lost}	$V_{lost} = (\Delta_n * M_{Hal}) / \rho_{Hal}$	6.14E-05	m^3
Subrosion rate, $R_{m/yr}$	$R_{m/yr} = V_{lost} / (S_{cell} * \Delta t)$	6.14E-08	m/yr
Subrosion rate, $R_{mm/yr}$	$R_{mm/yr} = R_{m/yr} * 1000$	6.14E-05	mm/yr
Subrosion rate, $R_{m/Myr}$	$R_{m/Myr} = R_{m/yr} * 1,000,000$	0.06136	m/Myr
Subrosion rate, $R_{cm/Myr}$	$R_{cm/Myr} = R_{m/Myr} * 100$	6.13	cm/Myr
Water Volume, V_{wL}	$V_{wL} = V_w * 1000$	1	L
Darcy Flux (q) [m/yr]	**Batch volume (m2)**	**Batch volume (L or kg)**	
1.00E-06	0.001	1	
5.00E-05	0.05	50	
5.00E-04	0.5	500	
5.00E-03	5	5000	

Table C: Example of a PHREEQC simulation, testing with a Dacry flux $q = 1 * 10^{-6}$ *m/yr, and an inflow water composition of salinity 1 g/L. The caprock in this run is 13 meters thick and has a porosity of 1%. This outlines the calculations the software is running, from the amount of Halite moles removed from*

the system after a simulation of 1 year. Additionally, the water mass used for each Darcy flux is included in this table.

Link of the files for Petrel Seismic Interpreation and Phreeqc simulations:
https://surfdrive.surf.nl/s/TDyZmSkK4L8Eztj